Molecular Cell

Article

BLM and BRCA1-BARD1 coordinate complementary mechanisms of joint DNA molecule resolution

Graphical abstract

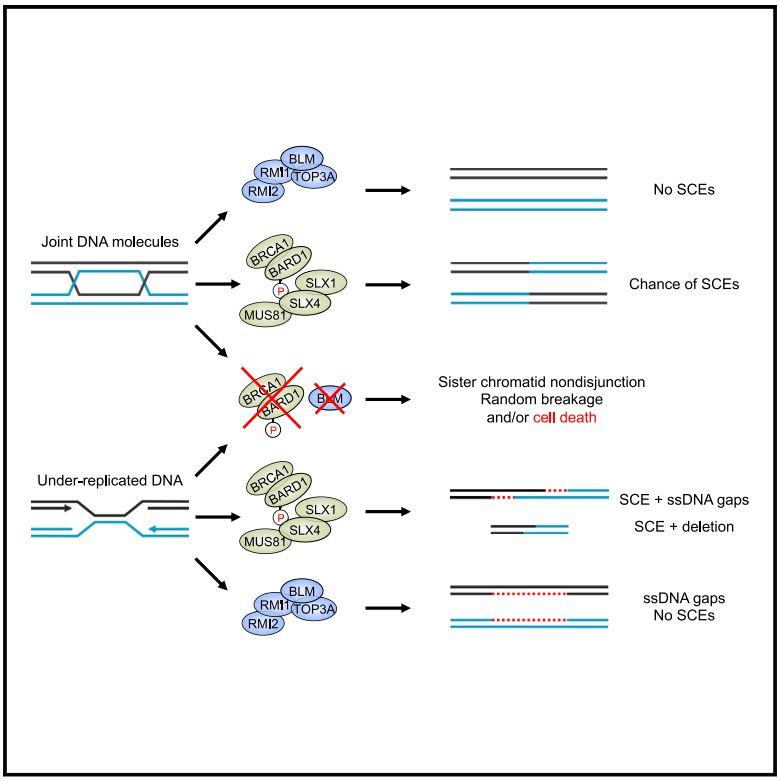

Highlights

- RECQL5 counteracts RAD51 filament formation, but BLM does not
- Combined deficiency in BLM and BRCA1-BARD1 (but not BRCA2) is synthetic lethal
- BARD1 recruits SLX4 and MUS81 to resolve DNA intermediates left unprocessed by BLM
- The phosphorylated BARD1 MUSIC motif interacts with SLX4 in a CDK1-dependent manner

Authors

Kaima Tsukada, Samuel E. Jones, Julius Bannister, ..., Benedikt M. Kessler, J. Ross Chapman, Andrew N. Blackford

Correspondence

andrew.blackford@imm.ox.ac.uk

In brief

Tsukada et al. identify a negative genetic interaction between the BLM helicase and the BRCA1-BARD1 complex. They reveal that this is due to a previously overlooked role for BARD1 in recruiting the SLX4 structure-specific nuclease complex to resolve DNA intermediates and joint molecules left unprocessed by BLM prior to cell division.

Tsukada et al., 2024, Molecular Cell *84*, 640–658
February 15, 2024 © 2023 The Authors. Published by Elsevier Inc.
https://doi.org/10.1016/j.molcel.2023.12.040

CellPress

CellPress
OPEN ACCESS

Molecular Cell

Article

BLM and BRCA1-BARD1 coordinate complementary mechanisms of joint DNA molecule resolution

Kaima Tsukada,[1,5] Samuel E. Jones,[1,5] Julius Bannister,[1] Mary-Anne Durin,[2] Iolanda Vendrell,[3,4] Matthew Fawkes,[1] Roman Fischer,[3,4] Benedikt M. Kessler,[3,4] J. Ross Chapman,[2] and Andrew N. Blackford[1,6,*]
[1]Department of Oncology, MRC Weatherall Institute of Molecular Medicine, University of Oxford, John Radcliffe Hospital, Oxford OX3 9DS, UK
[2]MRC Haematology Unit, MRC Weatherall Institute of Molecular Medicine, University of Oxford, John Radcliffe Hospital, Oxford OX3 9DS, UK
[3]Target Discovery Institute, Centre for Medicines Discovery, Nuffield Department of Medicine, University of Oxford, Oxford OX3 7FZ, UK
[4]Chinese Academy for Medical Sciences Oxford Institute, Nuffield Department of Medicine, University of Oxford, Oxford OX3 7FZ, UK
[5]These authors contributed equally
[6]Lead contact
*Correspondence: andrew.blackford@imm.ox.ac.uk
https://doi.org/10.1016/j.molcel.2023.12.040

SUMMARY

The Bloom syndrome helicase BLM interacts with topoisomerase IIIα (TOP3A), RMI1, and RMI2 to form the BTR complex, which dissolves double Holliday junctions and DNA replication intermediates to promote sister chromatid disjunction before cell division. In its absence, structure-specific nucleases like the SMX complex (comprising SLX1-SLX4, MUS81-EME1, and XPF-ERCC1) can cleave joint DNA molecules instead, but cells deficient in both BTR and SMX are not viable. Here, we identify a negative genetic interaction between BLM loss and deficiency in the BRCA1-BARD1 tumor suppressor complex. We show that this is due to a previously overlooked role for BARD1 in recruiting SLX4 to resolve DNA intermediates left unprocessed by BLM in the preceding interphase. Consequently, cells with defective BLM and BRCA1-BARD1 accumulate catastrophic levels of chromosome breakage and micronucleation, leading to cell death. Thus, we reveal mechanistic insights into SLX4 recruitment to DNA lesions, with potential clinical implications for treating BRCA1-deficient tumors.

INTRODUCTION

Homologous recombination (HR) is used to repair DNA double-strand breaks (DSBs) and maintain genome stability during DNA replication.[1] HR is initiated by resection of DNA ends to produce single-stranded DNA (ssDNA) overhangs, which recruit the RAD51 recombinase in a manner dependent on the tumor suppressors BRCA1 and BRCA2.[2] The RAD51 nucleoprotein filament then catalyzes strand invasion to form a displacement loop (D-loop) intermediate, which allows DNA synthesis from a homologous template to restore the broken chromosome.[3] The invading strand can then be displaced, and repair completed via synthesis-dependent strand annealing (SDSA).[4] Alternatively, second-end capture can occur, where the second, non-invading DSB end anneals to the displaced strand from the homologous template being used for repair, resulting in the formation of a double Holliday junction (dHJ). These and other joint DNA molecules can be highly toxic if they are not disassembled prior to cell division.[5]

dHJs can be removed by two genetically and biochemically distinct pathways, termed dissolution and resolution. dHJ dissolution is carried out by the Bloom syndrome helicase BLM in complex with topoisomerase IIIα (TOP3A) and two structurally related subunits, RMI1 and RMI2 (the BTR complex).[6] BLM helicase activity promotes convergent branch migration to create a hemicatenane structure, followed by decatenation catalyzed by TOP3A to dissolve the dHJ, which results exclusively in non-crossover DNA repair products.[7] Notably, mutations in BLM and other members of the BTR complex cause Bloom syndrome and related disorders in humans, with symptoms that include microcephaly, short stature, immunodeficiency, hypersensitivity to sunlight, and a greatly increased predisposition to a broad range of cancers.[8–10] Cells derived from Bloom syndrome patients commonly display multiple signatures of genome instability including elevated chromosomal aberrations and an up to ten-fold increase in sister chromatid exchanges (SCEs). However, it is still unclear which of the phenotypes of Bloom syndrome are specifically due to defects in dHJ dissolution, as BLM also maintains genome stability via other mechanisms such as promoting DNA-end resection (with DNA2[11–13]), processing ultrafine DNA bridges (UFBs) in anaphase (with PICH[14,15]), and restarting stalled replication forks (with RPA[16,17]).

In contrast to dissolution, dHJ resolution involves DNA cleavage by structure-specific endonucleases, either the SMX complex (comprising SLX1-SLX4, MUS81-EME1, and XPF-ERCC1)

 © 2023 The Authors. Published by Elsevier Inc.
This is an open access article under the CC BY license (http://creativecommons.org/licenses/by/4.0/).

CellPress
OPEN ACCESS

or GEN1.[18–27] However, given that dHJ resolution can produce both crossover and non-crossover products, dissolution by BTR is presumably favored over resolution by SMX or GEN1 to avoid the potential for loss of heterozygosity, which is likely to increase the risk of cancer development in multicellular organisms. Nonetheless, the SMX complex plays vital roles in human cells, in particular in DNA interstrand crosslink repair,[28] as highlighted by the fact that biallelic mutations in SLX4 or XPF can cause Fanconi anemia, a disorder characterized by bone marrow failure and increased predisposition to some cancers.[29–32] In line with this, SLX4 recruitment to DNA interstrand crosslinks was shown to require FANCD2 and monoubiquitylation of the latter by the Fanconi anemia core complex.[33,34] However, in other experiments SLX4 localization was found to be FANCD2-independent,[35,36] indicating that multiple factors may recruit SLX4 to DNA lesions in a context-dependent manner.

Human cells lacking dHJ dissolution and resolution pathways are not viable, as they accumulate severe chromosomal aberrations and extensive DNA damage.[23,25,26,37] In line with this, prior studies in fission yeast,[38] budding yeast,[39] flies,[19,40,41] and worms,[42] all demonstrated synthetic lethality between orthologs of BLM and MUS81, SLX4, or GEN1. It is important to note that dHJs are not the only DNA intermediates that can be dealt with by these enzymes: D-loops, single HJs, late replication intermediates, and secondary DNA structures can also be substrates for BTR, SMX, and/or GEN1 to varying degrees.[5,43]

Here, we identify a negative genetic interaction between BLM and the BRCA1-BARD1 complex. We show that this is caused by loss of a previously uncharacterized but highly conserved peptide motif in BARD1, centered around serine 148. This motif controls a phospho-dependent functional interaction between BARD1 and SLX4 and is required for recruitment of SLX4 and MUS81 to mitotic DNA lesions, where it acts to prevent catastrophic chromosome breakage and micronucleation in cells lacking BLM.

RESULTS

No evidence for a role for BLM in regulating RAD51 in human cells

The role of BLM in dHJ dissolution is well established, but it is less clear to what extent BLM functions in regulating HR at the level of RAD51 filament formation. Some studies showed that RAD51 foci are reduced in BLM-deficient cells,[44–46] whereas others have reported either no defect,[17,47–49] or else elevated numbers of RAD51 foci in absence of BLM.[50,51] By contrast, previous studies agree that the BLM-related RecQ helicase RECQL5 plays a major role in counteracting RAD51 filament formation.[52–54]

To confirm the roles BLM and RECQL5 play in regulating RAD51 at DSBs in human cells, we generated Δ*BLM* and Δ*RECQL5* RPE-1 cells using CRISPR-Cas9 (Figure S1A). We then treated these cells with ionizing radiation (IR) and performed quantitative image-based cytometry (QIBC) to measure RAD51 foci formation in thousands of cells per timepoint (Figures S1B–S1D).[55] Results showed clearly that Δ*BLM* RPE-1 cells do not have a defect in RAD51 foci formation, nor do they display elevated RAD51 accumulation either before or after IR. By contrast, Δ*RECQL5* cells displayed elevated RAD51 foci at all time points before and after IR. Thus, these data support RECQL5 being the main RecQ helicase responsible for regulating HR by counteracting RAD51 filament assembly, rather than BLM.

Nonetheless, although RAD51 foci in wild-type (WT) mouse cells are unaffected by BLM status, loss of BLM in a BRCA1 hypomorphic background (*Brca1*$^{\Delta 11/\Delta 11}$) can partially restore RAD51 foci formation.[48] We therefore also examined the effect of BRCA1 depletion on RAD51 foci in Δ*BLM* and parental RPE-1 cells (Figures S1E–S1H). However, we saw no indication that loss of BLM influences the RAD51 foci formation defect of BRCA1-depleted cells.[56]

Cells deficient in BLM and BRCA1-BARD1 show synergistic growth defects

During the course of the experiments described above, we noticed what appeared to be a high rate of cell death in BRCA1-depleted Δ*BLM* cells. To quantify this, we first performed colony survival assays in WT and Δ*BLM* cells treated with either control small interfering RNAs (siRNAs) or siRNAs targeting BRCA1. Results from these assays demonstrated that there was indeed a significant reduction in colony outgrowth of cells deficient in both BLM and BRCA1 (Figures 1A and 1B). To confirm this, we performed reciprocal experiments in which we depleted BLM using siRNA in Δ*BRCA1* RPE-1 cells and obtained similar results (Figures 1C and S2A).

BRCA1 forms a heterodimeric complex with BARD1, and both proteins depend on each other for mutual stability.[57,58] We therefore also depleted BLM using siRNA from HCT116 cells expressing BARD1 tagged with an auxin-inducible degron (AID). Consistent with results in RPE-1 cells deficient in BLM and BRCA1, *BARD1*$^{AID/AID}$ HCT116 cells depleted of BARD1 and BLM showed significantly reduced colony survival (Figures 1D, S2B, and S2C).

Given the critical role of BRCA1 in HR,[59] we wished to establish whether other key HR factors involved in promoting RAD51 loading, such as BRCA2,[60,61] would also be essential for cell growth in absence of BLM. Therefore, we depleted BLM using two different siRNAs from H1299 cells that express shRNAs targeting BRCA1 or BRCA2 upon addition of doxycycline. Results from colony survival assays carried out with these cells demonstrated that although double depletion of BLM and BRCA1 caused the expected drop in colony outgrowth, double depletion of BLM and BRCA2 had only a very minor effect (Figures 1E, 1F, and S2D–S2F). Taken together, our results indicate that combined deficiency in BLM and either BRCA1 or BARD1 causes a synergistic growth defect, but this is not caused by loss of BRCA2-dependent RAD51 recruitment. In line with this, *BLM* was identified as a candidate gene required for survival of BRCA1- but not BRCA2-deficient cells in a recently reported CRISPR screen.[62]

Finally, we investigated whether the reduction in growth of cells deficient in BLM and BRCA1 was caused by increased cell death rather than other mechanisms such as cell cycle arrest, senescence, or cell adhesion defects. We therefore measured the level of apoptosis in WT and Δ*BLM* cells treated with control siRNAs or depleted of BRCA1, using caspase 3/7

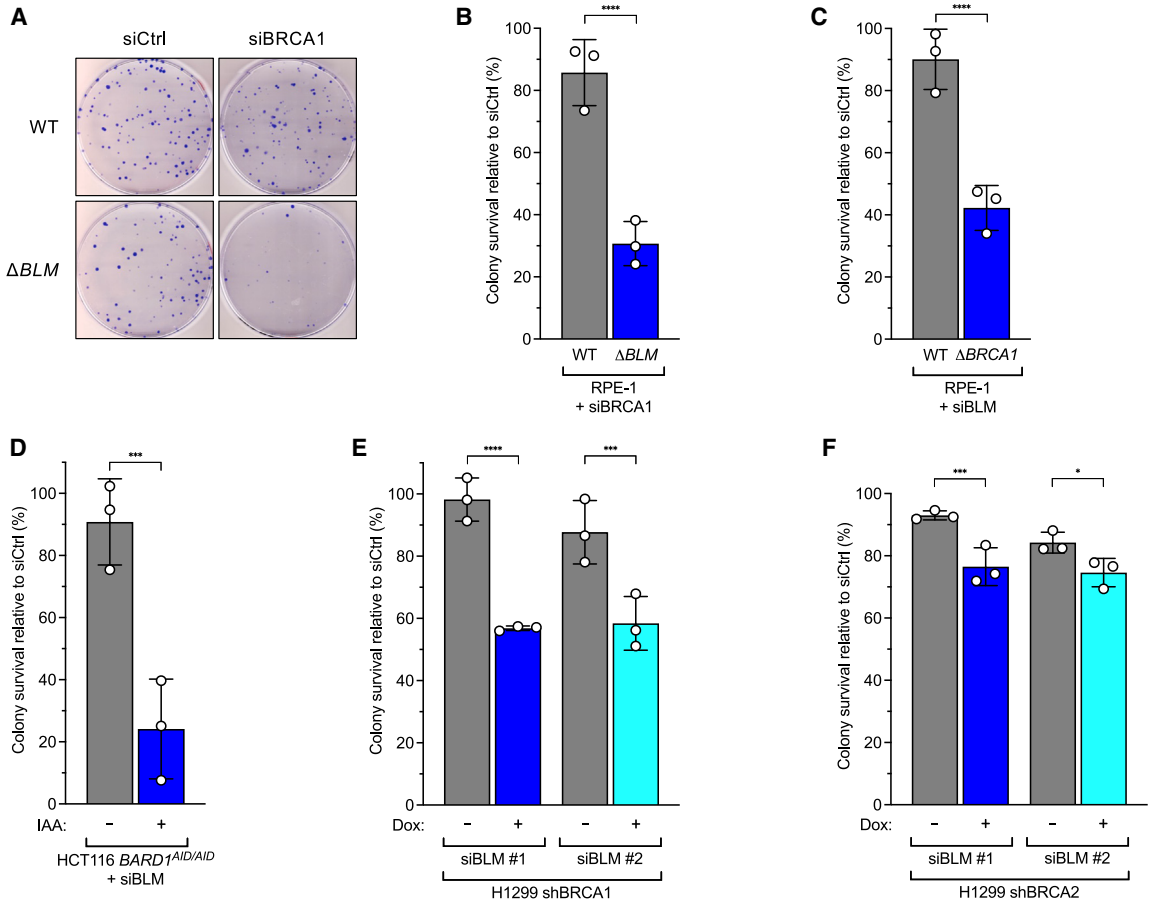

Figure 1. Loss of BLM causes cell death in BRCA1- but not BRCA2-deficient cells

(A) Representative images of colony survival assays with WT and Δ*BLM* RPE-1 FRT/TR Δ*TP53* cells treated with the indicated siRNAs.

(B) Quantification of the colony survival assays shown in (A). Error bars indicate standard deviation (SD) of n = 3 experiments.

(C) Quantification of colony survival assays with WT or Δ*BRCA1* RPE-1 FRT/TR Δ*TP53* cells treated with the indicated siRNAs. Error bars indicate SD of n = 3 experiments.

(D) Quantification of colony survival assays with HCT116 *BARD1*$^{AID/AID}$ cells treated with the indicated siRNAs. Cells were treated with 1 mM of the auxin indole-3-acetic acid (IAA) for 72 h, where indicated. Error bars indicate SD of n = 3 experiments.

(E) Quantification of colony survival assays with H1299 shBRCA1 cells treated with the indicated siRNAs. Cells were treated with 2 μg/ml doxycycline (Dox) 24 h before plating, where indicated. Error bars indicate SD of n = 3 experiments.

(F) Quantification of colony survival assays with H1299 shBRCA2 cells treated with the indicated siRNAs. Cells were treated with 2 μg/ml Dox 24 h before plating, where indicated. Error bars indicate SD of n = 3 experiments.

See also Figures S1 and S2.

cleavage as a readout.[63] Results from these experiments showed that although apoptosis levels were elevated slightly in BLM or BRCA1-deficient cells, there was a dramatic increase in cells deficient in both proteins (Figure 2A). We conclude from these data that increased cell death leads to the synergistic reduction in growth of cells deficient in BLM and BRCA1.

Cells deficient in BLM and BRCA1 accumulate DNA damage, chromosomal abnormalities, and micronuclei

BLM and BRCA1 both function at various stages of HR.[2,6] We therefore wanted to establish whether cells deficient in both proteins were dying from DNA damage. To this end, we examined levels of the DSB signaling markers γH2AX by flow cytometry and phosphorylated KAP1 by western blotting in WT and Δ*BLM* cells treated with either control siRNAs or siRNAs targeting BRCA1 in the absence of exogenous genotoxic stress (Figures 2B and 2C). Strikingly, γH2AX and KAP1-pS824 levels were elevated in cells deficient in both BLM and BRCA1, indicating an increased number of unrepaired DNA breaks. We also observed an extremely high rate of micronucleation in BRCA1-depleted Δ*BLM* cells (Figures 2D and 2E), indicating either a defect in chromosome segregation or increased chromosome breakage producing acentric fragments. Using CREST immunostaining to detect the presence of kinetochores,[64] we determined that the vast majority of micronuclei in BRCA1-depleted Δ*BLM* cells derive from acentric fragments because they were CREST-negative (Figure 2F). In line with this, chromosome spreads prepared from such cells showed

CellPress
OPEN ACCESS

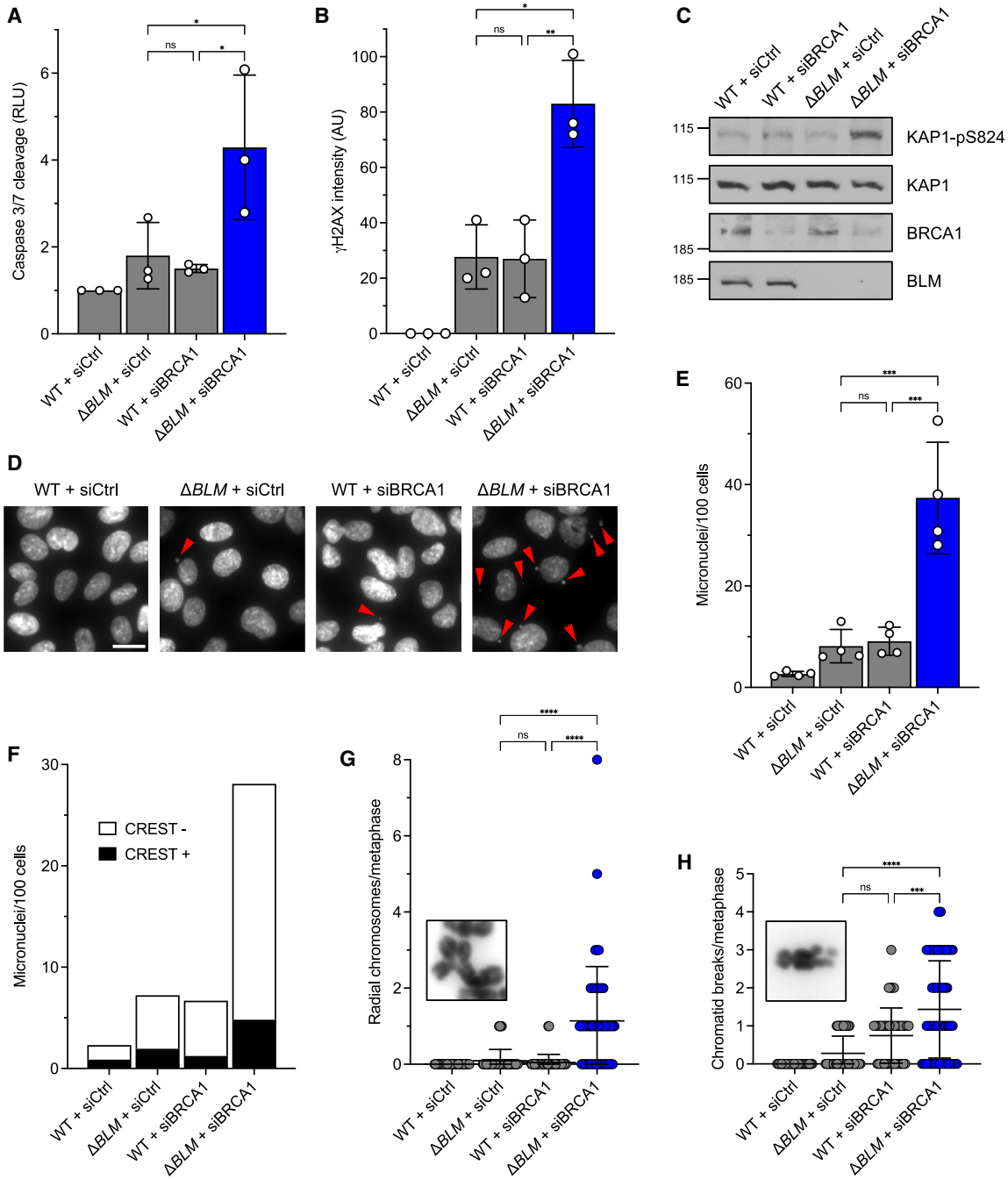

Figure 2. Cells deficient in BLM and BRCA1 accumulate DNA damage, chromosomal abnormalities, and micronuclei

(A) Quantification of caspase 3/7 cleavage levels as an indirect readout of apoptosis in WT and Δ*BLM* RPE-1 FRT/TR Δ*TP53* cells treated with the indicated siRNAs. Error bars denote SD from n = 3 experiments. RLUs, relative luminescence units. Two-way ANOVA followed by Tukey's post hoc test was used to calculate significance.

(B) Quantification of γH2AX levels by flow cytometry in WT and Δ*BLM* RPE-1 FRT/TR Δ*TP53* cells treated with the indicated siRNAs. Error bars denote SD from n = 3 experiments. AUs, arbitrary units. Two-way ANOVA followed by Tukey's post hoc test was used to calculate significance.

(C) Western blots of lysates from WT and Δ*BLM* RPE-1 FRT/TR Δ*TP53* cells treated with the indicated siRNAs.

(D) Representative images of micronuclei formation in WT and Δ*BLM* RPE-1 FRT/TR Δ*TP53* cells treated with the indicated siRNAs. Nuclei and micronuclei are stained with DAPI. Micronuclei are highlighted with red arrows. Scale bars, 100 μm.

(legend continued on next page)

that they accumulated a significantly higher number of chromatid breaks, as well as radial chromosomes (Figures 2G and 2H). These data suggest that chromosome breakage and rampant micronucleation are likely to be the main driver of cell death in absence of BLM and BRCA1.

BRCA1-deficient cells require BLM helicase activity and an intact BTR complex for survival

BLM helicase activity and interaction with TOP3A and RMI1 to form the BTR complex are important for some or possibly all of its cellular functions.[6] We therefore wished to test whether they also contribute to survival of BRCA1-deficient cells. To this end, we used lentiviral transduction to complement Δ*BLM* RPE-1 cells with either GFP or GFP-tagged BLM^{WT}, BLM^{K695R}, or $BLM^{\Delta TR}$ (Figures 3A and S3A). The K695R mutation inactivates the helicase domain of BLM,[65] whereas ΔTR is a deletion of amino acid residues 4–37 in the BLM N terminus that prevents interaction with TOP3A and RMI1.[17] Although expression of GFP-BLM^{WT} restored survival of BRCA1-depleted Δ*BLM* cells back to WT levels, neither mutant protein could (Figure 3B). Notably, although Δ*BLM* cells expressing BLM^{K695R} remained severely sensitive to depletion of BRCA1, the survival of cells complemented with the $BLM^{\Delta TR}$ protein was intermediate between WT and Δ*BLM*. This is in line with previous work demonstrating that loss of BLM helicase activity is equivalent to having no BLM at all, whereas loss of stable interaction between BLM and TOP3A-RMI1 causes hypomorphic phenotypes.[66] Nonetheless, these data suggest that both BLM helicase activity and BLM association with the BTR complex are important for survival of BRCA1-deficient cells.

To confirm the importance of an intact BTR complex if BRCA1 is absent, we depleted RMI1 and TOP3A from WT and Δ*BRCA1* RPE-1 cells with two different siRNAs per gene and performed further survival assays (Figures 3C and S3B). Results showed that depletion of these factors caused a synergistic drop in survival in BRCA1-deficient cells compared with their WT parental controls. These data are in line with the requirement for stable interaction of BLM with TOP3A-RMI1 and demonstrate that an intact BTR complex is crucial for survival of cells lacking BRCA1.

BRCA1-deficient tumors express higher levels of BTR complex components

Cancer cells with deficiencies in one biological pathway that come to rely more on a second pathway for survival are presumably far less likely to downregulate components of that second pathway. During tumor evolution, selection pressure may even produce cancer cells that upregulate factors involved in that second pathway. For example, HR-deficient tumors that depend on alternative end-joining for survival commonly upregulate *POLQ* expression.[67] We therefore wondered whether the negative genetic relationship between BRCA1 and components of the BTR complex might be apparent from analyses of human tumor samples. To this end, we compared expression of BTR components in BRCA1-proficient and BRCA1-deficient patient samples from The Cancer Genome Atlas (TCGA). Results from these analyses showed significantly increased expression of *BLM*, *RMI1*, and *RMI2* in BRCA1-deficient tumor samples (Figure 3D), in support of the idea that cells with pathogenic mutations in BRCA1 are more reliant on the BTR complex for survival. By contrast, higher *TOP3A* expression levels did not appear to correlate with BRCA1 deficiency; this may be because *TOP3A* is an essential gene in proliferating cells, unlike other members of the BTR complex.[68–70] Finally, and in line with the lack of a genetic interaction between BLM and BRCA2 (Figure 1F), we observed no significant increase in *BLM* expression in samples with loss-of-function mutations in *BRCA2* (Figure S3C).

BRCA1-deficient cells depend on EXO1 but not PICH for survival

In addition to promoting dHJ dissolution and suppressing SCEs, BLM is also implicated in DNA-end resection and plays a key role in UFB resolution.[7,11,14,71] We therefore wished to establish whether either of these functions contributes to cell survival in absence of BRCA1. BLM is thought to cooperate with DNA2 in resection,[12,13] but we found that depletion of DNA2 was highly toxic to cells regardless of BRCA1 status (data not shown), possibly due to its role in Okazaki fragment processing during DNA replication.[72] We therefore resorted to testing the requirement for EXO1 for the viability of BRCA1-deficient cells, as EXO1 is the other major nuclease that promotes long-range DNA-end resection in human cells.[73] In parallel, we tested the requirement for PICH for survival in absence of BRCA1, as it cooperates with BLM in UFB processing.[14,15] EXO1 and PICH were depleted using siRNAs in WT and Δ*BRCA1* RPE-1 cells, and effects on cell survival were examined (Figures 3E and S3D). PICH depletion did not have a significant effect on survival of BRCA1-deficient cells, indicating that the role of BLM in UFB processing is no more important for survival in Δ*BRCA1* cells than in WT cells. By contrast, EXO1 depletion caused a significant drop in survival of Δ*BRCA1* cells compared with WT cells. This is in line with recent data suggesting that EXO1 but not PICH is important for survival in absence of BRCA1.[62,74] These results indicated that loss of BLM-dependent DNA-end resection might be responsible for the increase in cell death in BRCA1-deficient cells, especially as loss of the DNA-end resection factor CtIP is also synthetic lethal with BRCA1-BARD1 deficiency.[75,76]

To test this hypothesis, we reasoned that loss of 53BP1 would be expected to rescue the toxic effects of BLM or EXO1 depletion in Δ*BRCA1* cells, as 53BP1 acts to limit DNA-end resection and its removal rescues the PARP inhibitor hypersensitivity of

(E) Quantification of micronuclei in cells described in (D). Error bars denote SD from n = 4 experiments. Two-way ANOVA followed by Tukey's post hoc test was used to calculate significance.
(F) Quantification of CREST-positive and CREST-negative micronuclei in WT and Δ*BLM* RPE-1 FRT/TR Δ*TP53* cells treated with the indicated siRNAs.
(G) Quantification of radial chromosomes in WT and Δ*BLM* RPE-1 FRT/TR Δ*TP53* cells treated with the indicated siRNAs. Error bars denote SD from n = 3 experiments. Two-way ANOVA followed by Tukey's post hoc test was used to calculate significance.
(H) Quantification of chromatid breaks in WT and Δ*BLM* RPE-1 FRT/TR Δ*TP53* cells treated with the indicated siRNAs. Error bars denote SD from n = 3 experiments. Two-way ANOVA followed by Tukey's post hoc test was used to calculate significance.

CellPress
OPEN ACCESS

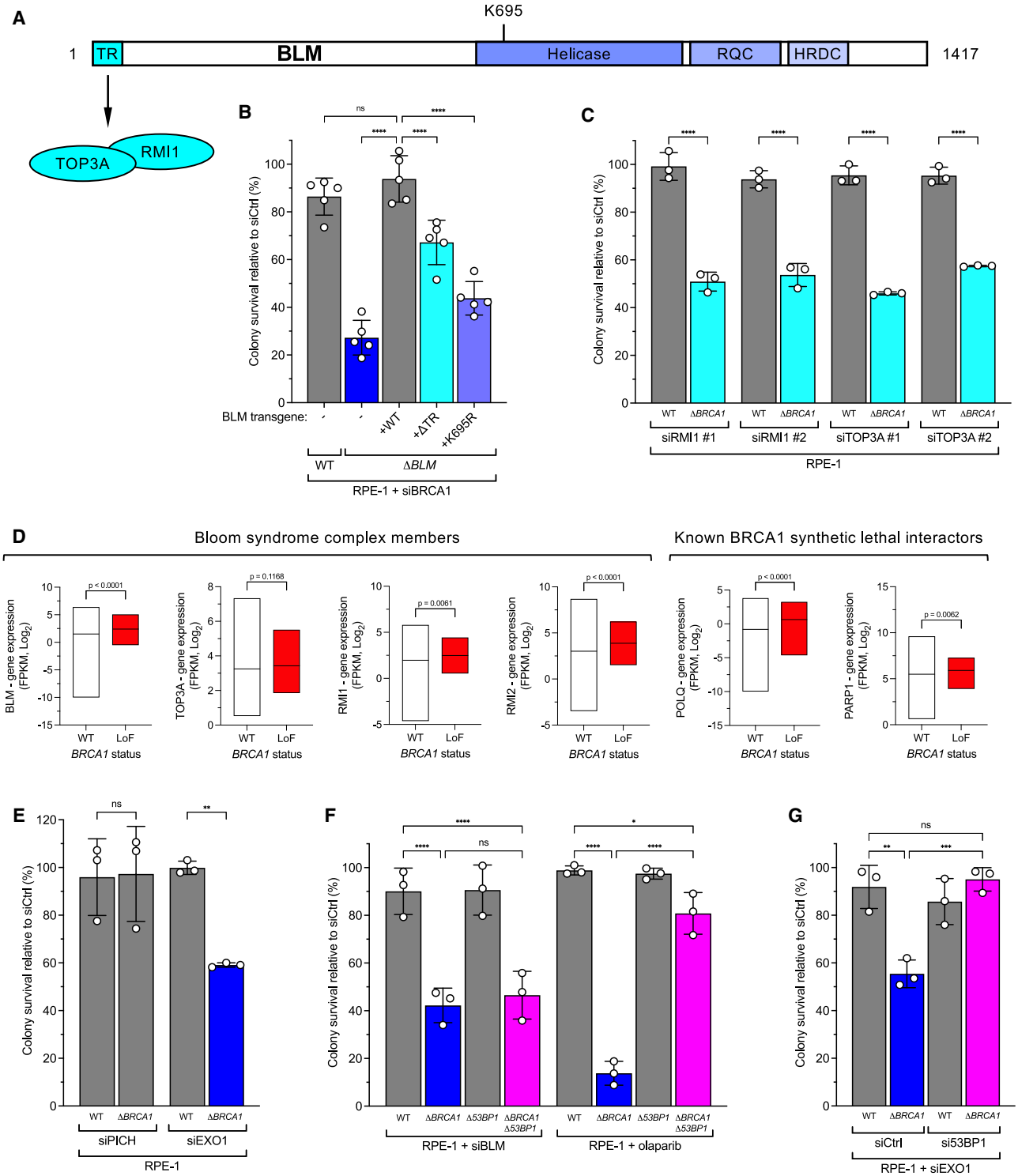

Figure 3. BRCA1-deficient cells depend on a functional BTR complex and EXO1 for survival

(A) Schematic of the human BLM protein showing the location of the TOP3A-RMI1 binding site at the N terminus and K695 in the helicase domain. TR, TOP3A-RMI1 binding domain; RQC, RecQ C-terminal domain; HRDC, helicase and RNaseD C-terminal domain.

(B) Quantification of colony survival assays with WT and Δ*BLM* RPE-1 FRT/TR Δ*TP53* cells treated with siCtrl or siBRCA1, and expressing the indicated GFP or GFP-BLM proteins. Error bars denote SD from n = 5 experiments.

(legend continued on next page)

BRCA1-deficient cells.[77] We therefore examined the effects of BLM or EXO1 depletion on survival of WT cells and cells deficient in BRCA1, 53BP1, or both (Figures 3F, 3G, S3E, and S3F). Results showed that the effect of EXO1 depletion on survival of BRCA1-deficient cells was indeed rescued by 53BP1 loss, but 53BP1 knockout had no effect on survival of cells deficient in BRCA1 and BLM. We therefore conclude firstly that BRCA1-deficient cell death upon BLM depletion is probably not caused by loss of BLM-dependent DNA-end resection. This is in line with our previous observations that BLM-deficient cells show only mild defects in resection.[17] Secondly, we conclude that the mechanistic basis of synthetic sickness caused by loss of EXO1 in BRCA1-deficient cells is fundamentally different from that caused by loss of BLM. We did not explore the genetic relationship between BRCA1 and EXO1 further; indeed, this has been explored in detail by van de Kooij et al. in a complementary study.[74]

BLM-deficient cells depend on multiple conserved domains in BARD1 for survival

We next wished to establish which BRCA1-BARD1 functions maintain cell survival in absence of BLM to gain insight into the underlying mechanistic basis for the synthetic growth defect. We therefore carried out extensive structure-function analyses of the BRCA1 and BARD1 proteins. BRCA1 has a highly conserved N-terminal RING domain (Figure 4A), which contains its BARD1 binding site.[57] The BRCA1 C terminus consists of a coiled-coil (CC) motif required for PALB2 binding,[78–80] and tandem BRCT domains that interact with multiple proteins including CtIP, FANCJ, and Abraxas.[81–84] To test whether these domains are required for survival of BLM-deficient cells, we complemented Δ*BRCA1* RPE-1 cells with GFP-tagged BRCA1^{WT}, BRCA1$^{\Delta CC}$, or BRCA1^{S1655A} via lentiviral transduction (Figure S4A; note that S1655A is a mutation that disrupts BRCT binding to phospho-peptide ligands[85–87]). We then treated these cells with siRNAs targeting BLM and assessed effects on colony survival (Figure 4B). Interestingly, both the BRCA1$^{\Delta CC}$ and BRCA1^{S1655A} mutants were fully able to complement the survival defects of siBLM-treated Δ*BRCA1* cells, even though they could not restore PARP inhibitor resistance (Figure S4B). These results are in line with our observation that BLM depletion from BRCA2-deficient cells does not confer a synthetic growth defect and thus confirm that BLM-deficient cells are not sensitive to BRCA1 loss because of its role in promoting HR with BRCA2, PALB2, and one or more of its BRCT domain binding partners.

Next, we carried out structure-function analyses of the evolutionarily conserved regions of the BARD1 protein (Figure 4C). BARD1 contains an N-terminal RING domain, which binds BRCA1 and contributes to E3 ubiquitin ligase activity of the BRCA1-BARD1 heterodimer. The BARD1^{R99E} mutation inhibits E3 ligase activity,[89] which is required for male fertility but not for HR.[90–93] The BARD1 C terminus comprises a chromatin recruitment module consisting of an ankyrin repeat domain (ARD), which recognizes the H4K20me0 mark, and tandem BRCT domains, which contain a ubiquitin-binding recruitment motif that recognizes H2AK15ub. Both the ARD and BRCTs are essential for BRCA1-BARD1 recruitment to damaged chromatin in S phase and for BRCA1-dependent HR.[92,94,95] The BARD1 BRCTs also contain residues to bind phospho-peptides (e.g., Lys619), but as yet no phospho-dependent binding partner has been identified. However, although the K619A mutation that would be predicted to abolish phospho-peptide binding ability does not cause an HR defect,[92] it does cause a nascent ssDNA degradation phenotype upon replication stress.[96] Finally, BARD1 also contains a short linear peptide motif downstream of the RING domain centered around Ser148 that is poorly characterized but highly conserved in vertebrate BARD1 orthologs (Figure 4D) and likely to be phosphorylated by CDK1.[97,98]

To investigate which domains of BARD1 are important for survival of BLM-deficient cells, we depleted BLM from *BARD1*$^{AID/AID}$ HCT116 cells treated with auxin and stably expressing either BARD1^{WT} or BARD1^{R99E}, BARD1^{S148A}, BARD1$^{ARD\text{-}3A}$, BARD1^{K619A}, or BARD1^{D712A} mutants (Figures S4C and S4D) and carried out colony survival assays (Figure 4E). Results demonstrated that neither the R99E nor the K619A mutant caused a survival defect upon BLM depletion, indicating that loss of BRCA1-BARD1 E3 ligase activity or increased nascent ssDNA degradation do not drive cell death in absence of BLM. By contrast, expression of the ARD (ARD-3A) and ubiquitin-dependent recruitment (D712A) mutants did not support survival of BLM-depleted cells, indicating that localization of BRCA1-BARD1 to DNA lesions is critical in absence of BLM. Finally, we also observed a significant drop in survival of BLM-deficient cells upon expression of the BARD1^{S148A} mutant, which for this reason we decided to pursue further.

Identification of a novel SMX-binding motif in BARD1

AlphaFold[99,100] predictions of the structure of full-length BARD1 suggested that despite its proximity to the RING domain, the Ser148 motif is discrete and does not contact the RING or any other part of BARD1 (Figure 5A). A β-hairpin was predicted with medium- to high-level confidence (predicted local distance difference test [pLDDT] ~50–90) to form around Ser148 (Figure S5A), in contrast to the low-confidence (pLDDT < 50)

(C) Quantification of colony survival assays with WT and Δ*BRCA1* RPE-1 FRT/TR Δ*TP53* cells treated with the indicated siRNAs. Error bars denote SD from n = 3 experiments.
(D) TCGA dataset analyses showing expression levels of BLM-TOP3A-RMI1-RMI2 complex members in BRCA1-proficient tumors or tumors with loss-of-function mutations in BRCA1. Two-tailed Welch's unpaired t-test was applied to calculate significance.
(E) Quantification of colony survival assays with WT and Δ*BRCA1* RPE-1 FRT/TR Δ*TP53* cells treated with the indicated siRNAs. Error bars denote SD from n = 3 experiments.
(F) Quantification of colony survival assays with WT, Δ*BRCA1*, Δ*TP53BP1*, and Δ*BRCA1*/Δ*TP53BP1* RPE-1 FRT/TR Δ*TP53* cells treated with the indicated siRNAs. Error bars denote SD from n = 3 experiments.
(G) Quantification of colony survival assays with WT and Δ*BRCA1* RPE-1 FRT/TR Δ*TP53* cells treated with the indicated siRNAs. Error bars denote SD from n = 3 experiments.
See also Figure S3.

CellPress
OPEN ACCESS

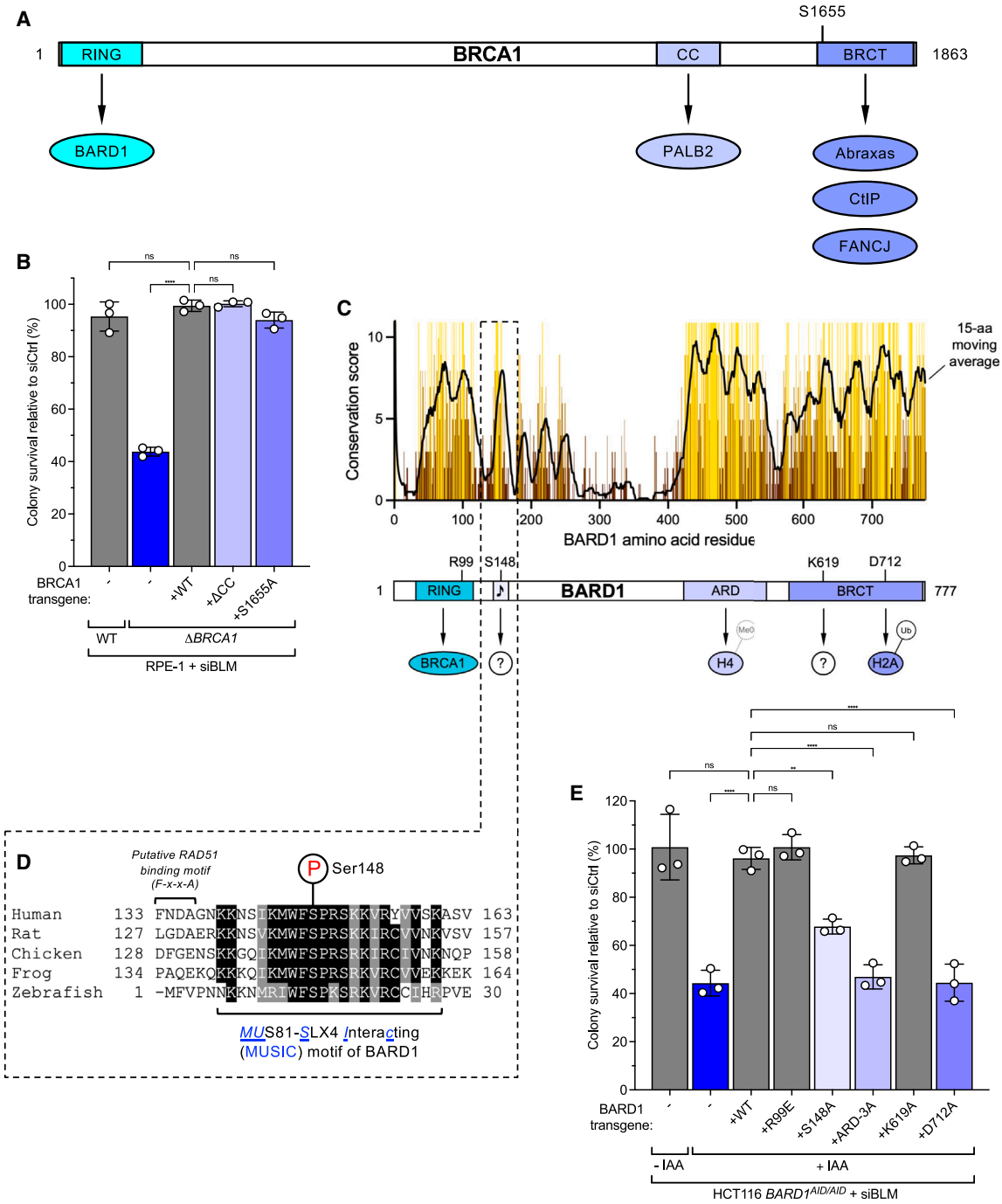

Figure 4. Structure-function analyses of BRCA1 and BARD1 reveal motifs required for survival of BLM-deficient cells

(A) Schematic of the human BRCA1 protein showing its conserved domains, protein binding partners, and the location of the S1655 residue, mutation of which inactivates phospho-peptide binding by the tandem BRCT domain.

(B) Quantification of colony survival assays with WT and Δ*BRCA1* RPE-1 FRT/TR Δ*TP53* cells treated with siCtrl or siBLM, and expressing the indicated BRCA1 proteins. Error bars denote SD from n = 3 experiments.

(C) Schematic of the human BARD1 protein showing its conserved domains, binding partners, and the location of the mutations used in (E). The heatmap was generated using ClustalO and Jalview. The degree of conservation of individual residues is indicated by height (ClustalO consensus) and color (BLOSUM62 score; yellow, high; brown, low).

(legend continued on next page)

predictions usually associated with disordered regions. Circular dichroism spectroscopy provided experimental support for this and indicated that phosphorylation of Ser148 does not affect the overall secondary structure (Figure S5B). These predictions indicated to us that the Ser148 motif could be a novel binding site for an as-yet unidentified interaction partner for BARD1.

To investigate this possibility, we designed two synthetic biotinylated peptides corresponding to the residues surrounding Ser148, one containing a phospho-serine at this residue and the other being the native peptide. These peptides were conjugated to streptavidin-coupled beads and incubated in HeLa nuclear extracts, and potential interacting partners were identified from two independent experiments by liquid chromatography-tandem mass spectrometry (LC-MS/MS; Table S1). Strikingly, when we examined proteins enriched in the phospho-BARD1 peptide pull-downs, we identified core components of the SMX complex, including MUS81, EME1, SLX4, SLX4IP, and XPF (Figures 5B and 5C). ERCC1 was also present and enriched, though only in one of the two experimental replicates. Given that synthetic lethality between loss of orthologs of BLM and SMX components has been observed from yeast to humans, the SMX complex seemed like a plausible binding partner for a motif in BARD1 that BLM-deficient cells depend on for survival. This idea is also supported by recent studies that identified SMX components in association with BRCA1.[101–105]

To verify whether full-length BARD1 could interact with the SMX complex and its dependence on Ser148, we carried out immunoprecipitations from extracts from cells transfected with plasmids encoding Spot-tagged BARD1^{WT} or BARD1^{S148A}. Results showed that although SLX4 and MUS81 were pulled down by the WT protein, the S148A protein could not do so above the background levels seen in the empty vector control (Figure 5D). As a further control, we also tested whether the BARD1-S148A mutation affected other protein-protein interactions of the BRCA1-BARD1 complex including those of BARD1 with BRCA1, PALB2, CtIP, FANCJ, Abraxas, and RAD51. As expected, there was no difference between BARD1^{WT} and BARD1^{S148A} in their interactions with these factors (Figure S5C), indicating that the S148A mutation does not cause a general defect in the ability of the BRCA1-BARD1 heterodimer to bind its interacting partners. This was particularly important to verify for RAD51 because Ser148 is located near a putative RAD51-binding motif in human BARD1 (although the critical F-x-x-A residues are not conserved in BARD1 orthologs; Figure 4D).[88]

Notably, we could only specifically detect the interaction between BARD1^{WT} and SMX components if these cells were pretreated with nocodazole, indicating that the interaction is maximal in G2/M cells when CDK1 is active. This is in line with previous reports indicating that Ser148 phosphorylation is CDK1-dependent.[97,98] Interestingly, in one of those reports an additional CDK1 phosphorylation site was identified in BARD1 at the Thr299 position.[97] However, in contrast to Ser148, Thr299 is poorly conserved in mammals and is absent in other vertebrates (Figure S5D). We also found that phospho-Thr299 peptides could not pull down SMX components (Figure S5E), perhaps not surprisingly as Thr299 and its surrounding residues do not resemble those surrounding Ser148 (Figure S5F). Taken together, these data confirm that BRCA1-BARD1 interacts with the SMX complex in a manner dependent on phosphorylated Ser148 of BARD1. We therefore refer to Ser148 and its surrounding residues as the MUS81-SLX4-interacting constituent (MUSIC) motif of BARD1.

The MUSIC motif of BARD1 interacts with the SMX complex via SLX4 in a CDK1-dependent manner

We wished to determine which component of SMX the MUSIC motif interacts with. SLX4 acts as a scaffold to bring together multiple structure-specific nucleases,[106] namely SLX1, MUS81-EME1, and XPF-ERCC1 (the latter supported by an additional co-factor, SLX4IP; Figure 5C). We therefore carried out further pull-downs with the native and phosphorylated BARD1 MUSIC motif peptides from lysates of cells deficient in SLX1, MUS81, XPF, or SLX4 (Figures 5E and S5G–S5I). Strikingly, only SLX4 depletion resulted in complete loss of SMX component binding to the phosphorylated MUSIC motif peptide (Figure 5E). These results indicate that BARD1 most likely interacts with the SMX complex via its SLX4 component, either directly or via another SLX4-associated protein that is not MUS81, EME1, XPF, ERCC1, SLX4IP or SLX1.

To confirm the dependence of BARD1-SMX binding on CDK1 activity and to demonstrate the interaction in an orthogonal way to our Spot-tag immunoprecipitation approach (Figure 5D), we made use of a single-cell colocalization system where BARD1 fused to an mCherry-tagged *lac* repressor (LacR) is targeted to a chromosomal site with ~256 copies of the *lac* operator (*lacO*) sequence integrated, and recruitment of GFP-SLX4 can be assessed (Figure 5F). Consistent with the Spot-pull-downs, while mCherry-LacR-BARD1^{WT} could recruit GFP-SLX4 to the *lacO* array above the background level observed in cells expressing mCherry-LacR alone, the mCherry-LacR-BARD1^{S148A} protein could not (Figures 5G and 5H). Furthermore, upon treatment with CDK1 inhibitor RO-3306, GFP-SLX4 could no longer be recruited even in cells expressing mCherry-LacR-BARD1^{WT}. These results confirm that BARD1 interacts in a CDK1-dependent manner with SLX4, most likely mediated by CDK1-dependent phosphorylation of BARD1 on Ser148.

The MUSIC motif of BARD1 recruits SLX4 and MUS81 in mitosis

To elucidate the cellular function of BRCA1-BARD1 interaction with SLX4 and identify the cause of the synthetic sick relationship with BLM loss, we needed to characterize cells expressing the BARD1 S148A MUSIC motif mutant. To this end, we first carried out colony survival assays to test whether loss of

(D) Sequence alignment of the MUSIC motif in vertebrate BARD1 orthologs. Note that zebrafish BARD1 lacks a RING domain and, hence, is missing the first ~130 residues found in other orthologs. A previously reported putative RAD51-binding motif near the MUSIC motif is also highlighted.[88]
(E) Quantification of colony survival assays with HCT116 *BARD1*$^{AID/AID}$ cells treated with siCtrl or siBLM and expressing the indicated BARD1 proteins. Cells were treated with 1 mM IAA for 72 h to deplete endogenous BARD1. Error bars denote SD from n = 3 experiments.
See also Figure S4.

CellPress
OPEN ACCESS

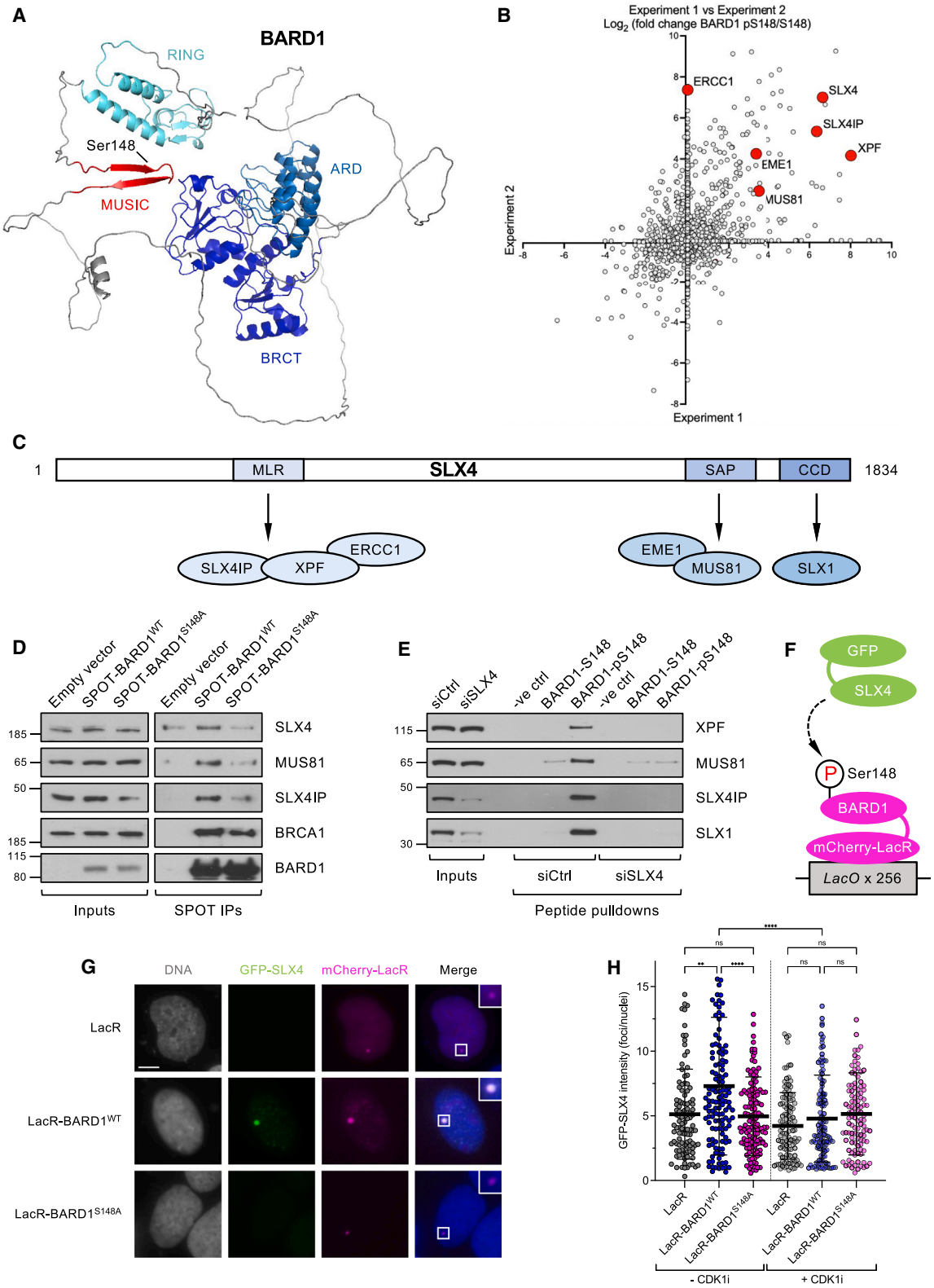

(legend on next page)

BARD1-SLX4 binding caused hypersensitivity to genotoxic stress (Figure 6A). Although cells expressing BARD1^{S148A} were not as sensitive to olaparib or cisplatin as BARD1-depleted cells, they nonetheless showed a substantial hypersensitivity to these agents compared with cells expressing BARD1^{WT}. This hypersensitivity was not caused by a defect in RAD51 loading, as cells expressing BARD1^{S148A} were as competent in RAD51 foci formation as cells expressing BARD1^{WT} (Figures 6B and 6C).

SLX1-SLX4 and MUS81-EME1 play important roles in cleaving dHJs, stalled replication forks, and other joint molecules to promote sister chromatid disjunction. Based on our findings above, we hypothesized that the BRCA1-BARD1 complex might be playing a previously uncharacterized role at the later stages of HR (after RAD51 loading and strand invasion) or at persistently stalled forks to recruit SLX1-SLX4 and MUS81-EME1 in order to cleave any remaining DNA entanglements that BLM cannot deal with before mitosis. If this model is right, then we would expect at least some of the increased SCEs in BLM-deficient cells to be dependent on Ser148 of BARD1. To test this, we knocked out *BLM* using CRISPR-Cas9 in *BARD1*$^{AID/AID}$ HCT116 cells, complemented them with BARD1^{WT} or BARD1^{S148A}, and then measured SCEs (Figures 6D and S6A). As expected, *BARD1*$^{AID/AID}$ Δ*BLM* cells displayed an extremely high rate of SCEs. Upon auxin treatment to deplete endogenous BARD1, SCEs were substantially reduced, also as expected due to the requirement for RAD51 in dHJ formation. Complementation of these cells with BARD1^{WT} restored the SCEs back to the high levels seen in Δ*BLM* cells. Strikingly, however, expression of BARD1^{S148A} was unable to do so, and SCEs remained significantly lower than in Δ*BLM* cells expressing BARD1^{WT}.

Our model predicts that a combination of BARD1-S148A mutation and MUS81 depletion would be epistatic in terms of decreasing SCEs in Δ*BLM* cells because they work together in the same pathway. Indeed, when we measured SCEs in Δ*BLM* cells expressing either BARD1^{WT} or BARD1^{S148A} and treated with control siRNAs or siRNAs targeting MUS81, this is exactly what we observed (Figures 6E and S6B). SCEs were highest in Δ*BLM* cells expressing BARD1^{WT} and MUS81, and expression of BARD1^{S148A} or MUS81 depletion both resulted in a decrease in SCEs. However, expression of BARD1^{S148A} in combination with MUS81 depletion in Δ*BLM* cells did not result in any additional decrease in SCEs compared with loss of MUS81 alone. These data support a model in which BARD1-dependent recruitment of the SMX complex is required to process HR or late replication intermediates that are missed by the BTR complex.

Finally, to demonstrate formally that SMX recruitment depends on BARD1 and an intact S148 motif, we examined SLX4 and MUS81 foci in early mitotic cells, when CDK1-dependent phosphorylation of SLX4 promotes MUS81-EME1 binding, assembly, and maximal nuclease activity of the SMX complex.[26,27,107–109] Due to lack of available antibodies specifically recognizing SLX4 by immunofluorescence, we produced WT and Δ*BLM* HCT116 *BARD1*$^{AID/AID}$ cells expressing GFP-SLX4 in a doxycycline-inducible manner (Figure S6C). In line with a backup role for SMX in dealing with joint molecules, we observed very few GFP-SLX4 or endogenous MUS81 foci in BLM-proficient cells (Figures 6F, 6G, and S6D–S6F). However, in BLM-deficient cells, we observed a significant increase in GFP-SLX4 and MUS81 foci in cells expressing BARD1^{WT}. Upon BARD1 depletion, these foci were reduced to background levels, in line with recent studies showing that loss of BRCA1-BARD1 leads to less SMX on chromatin.[101,103,110] Strikingly, BLM-deficient cells expressing BARD1^{S148A} were just as defective in their ability to recruit GFP-SLX4 and MUS81 to mitotic chromosomes as BARD1-depleted cells (Figures 6F, 6G, S6E, and S6F). Taken together, we thus establish that BARD1 promotes SLX4 and MUS81 recruitment to early mitotic chromosomes in a manner dependent on the MUSIC motif, where it likely deals with joint DNA molecules in a redundant manner with the BTR complex. Lack of this newly identified mechanism likely also explains the synergistic increase in cell death that results from combined deficiency in the BTR complex and BRCA1-BARD1.

DISCUSSION

We initiated this study to define the role of RecQ helicases in regulating RAD51 in human cells. The budding yeast RecQ ortholog Sgs1 is capable of disrupting Rad51 filaments.[111] Previous reports support a role for RECQL5 in RAD51 filament disassembly,[52–54] whereas others disagree on the relative importance of BLM in this process.[17,44–51] Our results confirm that RECQL5 is indeed required to limit RAD51 foci both before and after DNA

Figure 5. Identification of a novel MUS81-SLX4-interacting (MUSIC) motif in BARD1

(A) AlphaFold structure prediction of human BARD1 (UniProt A0AVN2), showing the expected location of the MUSIC motif and Ser148 in relation to the structured domains of BARD1.

(B) Scatter plot depicting $\log_2$-fold enrichment of BARD1-pS148 versus BARD1-S148 peptide-binding proteins from 2 independent experiments. See Table S1 for raw MS data. SMX subunits are highlighted in red.

(C) Schematic of the human SLX4 protein, showing which domains the other SMX components interact with. MLR, MUS312/MEI9 interaction-like region; SAP, SAF-A/B, Acinus, and PIAS; CCD, conserved C-terminal domain.

(D) Immunoprecipitations from lysates of 293FT cells transiently transfected with plasmids expressing Spot-tagged BARD1. Cells were treated with 100 ng/ml nocodazole for 16 h prior to harvesting.

(E) Pull-downs from lysates of 293FT cells treated with siCtrl or siSLX4 using biotinylated native or phosphorylated BARD1-Ser148 peptides. A peptide derived from RAD17 was used as a negative control.

(F) Schematic of the LacR/*lacO* assay using plasmid-encoded mCherry-LacR-fused BARD1 (or mCherry-LacR alone as a negative control; not shown) and GFP-tagged SLX4 transfected into a U2OS cell line containing ~256 *lacO* repeats.

(G) Representative images of the LacR/*lacO* assay in cells co-transfected with plasmids expressing GFP-SLX4 and either mCherry-LacR-fused BARD1^{WT}, mCherry-LacR-fused BARD1^{S148A}, or mCherry-LacR alone. Scale bars, 10 μm.

(H) Quantification of the LacR/*lacO* assay described in (G). Error bars denote SD from n = 3 experiments.

See also Figure S5.

CellPress
OPEN ACCESS

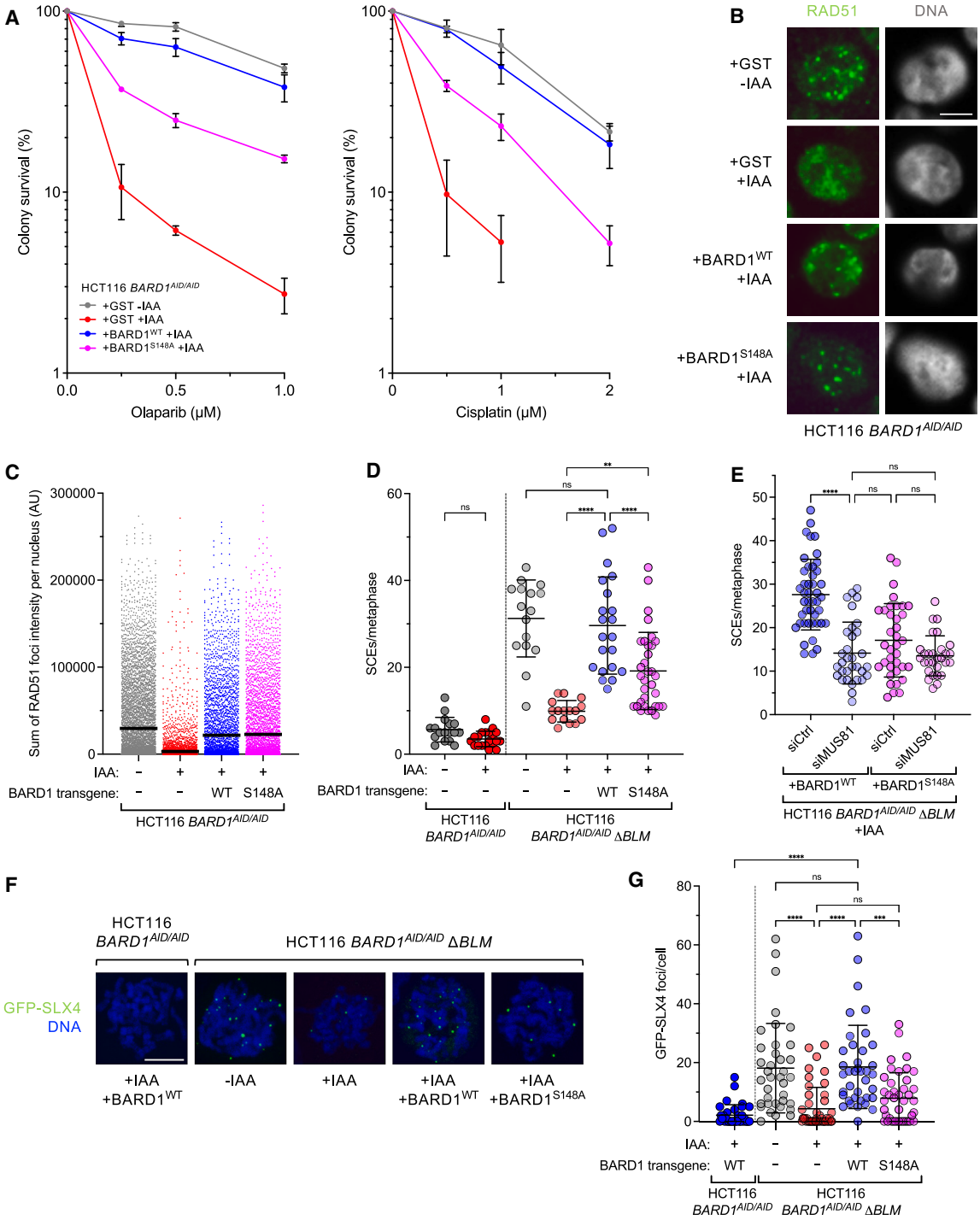

Figure 6. The BARD1-Ser148 motif recruits SLX4 to DNA lesions in mitosis

(A) Colony survival assays with HCT116 *BARD1*$^{AID/AID}$ cells expressing glutathione S-transferase (GST) or the indicated BARD1 proteins, treated with increasing doses of olaparib or cisplatin for 72 h. Error bars denote SD from n = 3 experiments.

(B) Representative images of RAD51 foci formation examined by immunofluorescence in HCT116 *BARD1*$^{AID/AID}$ cells expressing GST or the indicated BARD1 proteins. Cells were mock-irradiated or treated with 1 Gy IR before fixing after 2 h. DNA was stained with DAPI. Scale bars, 10 μm.

(C) Quantification of the sum of the intensities of RAD51 foci per nucleus, derived from QIBC analyses of n = 2 replicates. Cells were gated by DAPI intensity to include only S and G2 cells. Medians are shown as black bars. AU, arbitrary units.

(D) Quantification of SCEs in WT and Δ*BLM* HCT116 *BARD1*$^{AID/AID}$ cells expressing GFP or the indicated BARD1 proteins. Error bars denote SD from n = 3 replicates.

(legend continued on next page)

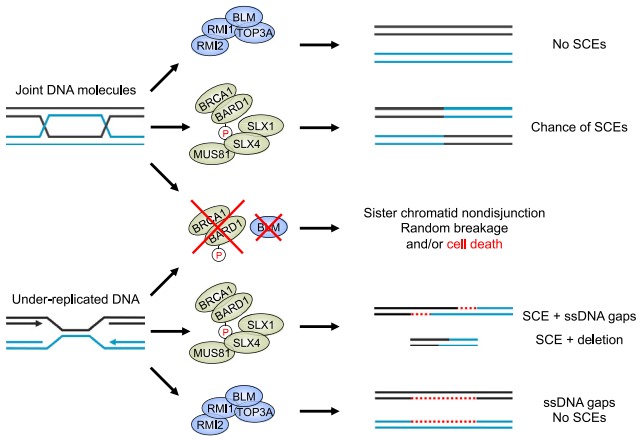

Figure 7. Model for the role of BRCA1-BARD1 binding to the SMX complex and the underlying mechanism for its synthetic sickness with BLM when both are deficient

See main text for details.

damage, whereas BLM is not (Figures S1B and S1C). This is in line with the fact that Sgs1 and RECQL5 both contain a conserved RAD51-binding BRCv motif required for filament disassembly,[112] which appears to be absent in BLM.

During our studies investigating a role for BLM in regulating RAD51, we discovered that loss of BLM in the context of BRCA1-BARD1 deficiency causes a synergistic growth defect in human cells. This negative genetic interaction can be explained by our finding that an evolutionarily conserved motif centered around Ser148 in BARD1 that we call the MUSIC motif, constitutes a binding site for SLX4 and its associated nucleases, which when mutated prevents their recruitment to joint DNA molecules. BLM loss combined with SLX4 or MUS81 inactivation has long been known to be synthetic lethal in organisms from yeast to humans.[19,23,25,26,38–42] In line with this, loss of BARD1-Ser148 causes increased cell death in absence of BLM, and we therefore hypothesize that a defect in SLX4 recruitment combined with loss of BTR-dependent processing of joint DNA molecules and/or late replication intermediates prevents sister chromatid disjunction during mitosis, leading to chromosome breakage, rampant micronucleation, and ultimately cell death.

It is interesting to note that a recent biochemical study using recombinant proteins demonstrated that although the BTR complex can efficiently dissolve dHJs regardless of whether they are chromatinized, the dHJ resolution activity of the SMX complex is significantly inhibited by chromatin.[113] This indicates that one or more additional factors must be required *in vivo* for SMX to resolve dHJs and presumably other DNA substrates. We propose that one of these factors is likely to be the BRCA1-BARD1 complex, which could act as a stable platform to position SMX in proximity to potential substrates, thus increasing its cutting efficiency. Alternatively, or in addition, BRCA1-BARD1 could play a more direct role in the nucleolytic reaction catalyzed by SMX. Future studies with purified recombinant proteins will be able to address this question.

In conclusion, we propose the following model (Figure 7). In contrast to the situation in yeast, recent work suggests that in human cells, the BTR complex remains active until the early stages of mitosis rather than being confined to S/G2 cells, with its activity likely to be maximal in early prophase.[114] This gives the BTR complex the chance to dissolve most joint molecules and replication intermediates prior to cell division to avoid crossovers and prevent loss of heterozygosity. However, BLM may not always catch all DNA entanglements before anaphase. We suggest that upon recruitment of BRCA1-BARD1 to DSB sites in S/G2 cells, RAD51 is loaded to promote error-free repair by HR. If any joint molecules are formed that BLM cannot deal with, BRCA1-BARD1 phosphorylation on Ser148 at the G2/M boundary (probably by CDK1[97,98]) would promote recruitment of SLX4 and nucleolytic cleavage of such DNA structures as a backup mechanism to promote cell division, although at the cost of potentially producing SCEs. Similarly, a region of under-replicated DNA could be unwound by the helicase activity of BLM and topological intertwines removed by TOP3A.[115] This would generate two daughter chromosomes, each with an ssDNA gap that would require gap-filling by a DNA polymerase while avoiding SCEs. Alternatively, a mutagenic pathway involving SLX4 recruitment by the BARD1 MUSIC motif could symmetrically cleave both leading strand templates to produce one intact daughter chromosome and two DSB ends that could be repaired by POLQ-mediated end-joining to produce a second daughter chromosome with a deletion.[116,117] SCEs would be produced in this case as well. Notably, it has long been known that BLM-deficient cells have a very high rate of SCEs as well as deletions and other chromosomal aberrations, which supports this model.[71,118] In mitotic cells where both the BTR complex and either BRCA1, BARD1, or BARD1 phosphorylation on Ser148 are defective, this would either lead to nondisjunction of sister chromatids or else random breakage events that produce acentric fragments, thereby leading to the high level of cell death that we have demonstrated in these cells.

The finding that loss of BLM causes cell death when combined with BRCA1 deficiency is of potential therapeutic relevance. Although PARP inhibitors have entered the clinic to treat BRCA-deficient tumors, drug resistance can rapidly develop.[77] One mechanism that BRCA1-deficient tumor cells can exploit is inactivation of the 53BP1 pathway.[119,120] We have found that although Δ*BRCA1*/Δ*TP53BP1* cells are indeed resistant to PARP inhibition, they are just as sensitive to BLM depletion as Δ*BRCA1* cells (Figure 3F). This raises the prospect of potentially utilizing BLM inhibitors to target a subset of BRCA1-deficient

(E) Quantification of SCEs in Δ*BLM* HCT116 *BARD1*$^{AID/AID}$ cells expressing BARD1^{WT} or BARD1^{S148A} and treated with the indicated siRNAs. Error bars denote SD from n = 2 replicates.

(F) Representative images of GFP-SLX4 foci in nocodazole-arrested WT or Δ*BLM* HCT116 *BARD1*$^{AID/AID}$ cells expressing the indicated BARD1 proteins after induction of GFP-SLX4 upon addition of Dox. Scale bars, 10 μm.

(G) Quantification of GFP-SLX4 foci in cells from (E). Error bars denote SD from n = 3 replicates.

See also Figure S6.

CellPress
OPEN ACCESS

cancers that have become resistant to PARP inhibitors. Of note, BLM inhibitors have been developed previously, although they are not yet suitable for use as drugs.[121,122]

Limitations of the study

Our data suggest that SLX4 (or an SLX4-associated protein that is not MUS81, EME1, XPF, ERCC1, SLX4IP, or SLX1) is the direct binding partner for the MUSIC motif of BARD1. Although SLX4 does not contain any known phospho-peptide binding domains, it is a large protein of 1834 residues, much of which is unstructured and poorly characterized. Future work will be needed to map the binding site of the BARD1 MUSIC motif on SLX4.

One final and major question arises from this work: what is the nature of the toxic DNA intermediates that cause cell death in cells deficient in BTR and BRCA1-BARD1? BLM knockout cells expressing BARD1^{S148A} (which are proficient in RAD51 loading; Figures 6B and 6C) have reduced SCEs (Figure 6D), suggesting that dHJ resolution is defective due to inefficient SLX4 recruitment in these cells. However, cells lacking BRCA1-BARD1 altogether (rather than just the SLX4-interacting motif) are HR-deficient, so dHJs may never accumulate regardless of the presence of BLM. Thus, we can envisage two possible scenarios to explain this: one, it is possible that dHJs still accumulate in cells lacking BLM and BRCA1 to some extent, as a result of RAD51-independent joint molecule formation, e.g., via RAD52.[123] Two, dHJs are not the only DNA substrate that BLM and the SMX complex are required to deal with—stalled replication forks, D-loops, late replication intermediates, and other potentially problematic secondary DNA structures could all be highly toxic if not processed in either a BTR- or SMX-dependent manner. Further work will be needed to address this.

STAR★METHODS

Detailed methods are provided in the online version of this paper and include the following:

- KEY RESOURCES TABLE
- RESOURCE AVAILABILITY
  - Lead contact
  - Materials availability
  - Data and code availability
- EXPERIMENTAL MODEL AND STUDY PARTICIPANT DETAILS
  - Cell lines and culture conditions
- METHOD DETAILS
  - RNA interference
  - Plasmids and cloning
  - Generation of knockout cells using CRISPR-Cas9
  - SDS-PAGE and western blotting
  - QIBC for RAD51 foci
  - Colony survival assays
  - Apoptosis assays
  - Flow cytometry
  - Micronuclei quantification
  - Analyses of chromosomal aberrations
  - Lentiviral transductions
  - TCGA analyses
  - Sequence alignments
  - Peptide pull-downs
  - Circular dichroism spectroscopy
  - Mass spectrometry
  - Immunoprecipitations
  - LacR/*lacO* single-cell colocalization assays
  - Sister chromatid exchange assays
  - Immunofluorescence and confocal microscopy
- QUANTIFICATION AND STATISTICAL ANALYSIS

SUPPLEMENTAL INFORMATION

Supplemental information can be found online at https://doi.org/10.1016/j.molcel.2023.12.040.

ACKNOWLEDGMENTS

We thank Richard Baer, Mirek Dundr, Daniel Durocher, Stephen Elledge, Roger Greenberg, Philip Hublitz, Stephen Jackson, John Rouse, Madalena Tarsounas, Stephen West, Feng Zhang, Eric Campeau, and Paul Kaufman for providing reagents and Sylvie Noordermeer and Haico van Attikum for helpful discussions prior to submission. Sarah Bonham and Ann-Marie Shorrocks carried out sample preparation prior to mass spectrometry and data analysis. We are grateful to Fena Ochs for help setting up QIBC and to David Staunton (Molecular Biophysics Suite, Department of Biochemistry, University of Oxford) for help with circular dichroism spectroscopy. The Blackford lab received funding from the University of Oxford Medical Sciences Internal Fund, the John Fell Oxford University Press Research Fund, and the Cancer Research UK (CRUK) Oxford Centre (C5255/A18085). A.N.B. was supported by fellowships from CRUK (C29215/A20772 and RCCSCF-May23/100001) and Against Breast Cancer/Oriel College. K.T. was supported by the Tokyo Tech Academy for Co-creative Education of Environment and Energy Science, the Tokyo Tech Academy for Leadership, a Grant-in-Aid Fellowship from the Japan Society for the Promotion of Science (JP20J13601), and a Japan Society for the Promotion of Science Overseas Research Fellowship. J.R.C. was supported by CRUK (RCCSCF-Nov21/100004) and by MRC Molecular Haematology Unit core funding in the form of a PhD studentship to M.-A.D. We would like to acknowledge Kevin Clark, Sally-Ann Clark, Paul Sopp, and Craig Waugh in the MRC Weatherall Institute of Molecular Medicine (WIMM) Flow Cytometry Facility for providing cell-sorting services; Jana Koth, the Wolfson Imaging Centre, and the Micron Advanced Bioimaging Facility for help with microscopy; and Ryan Beveridge in the MRC WIMM Virus Screening Facility for help in generation of lentiviral preparations. These facilities are supported by the MRC Molecular Haematology Unit (MC_UU_12009), the MRC Human Immunology Unit (MC_UU_12010), the Wolfson Foundation (18272), the Wellcome Trust (091911/B/10/Z and 107457/Z/15/Z), the National Institute for Health Research Oxford Biomedical Research Centre (IS-BRC-1215-20008), the CRUK Oxford Centre, the Kay Kendall Leukaemia Fund (KKL1057), the John Fell Fund (131/030 and 101/517), the EPA fund (CF182 and CF170), and the MRC WIMM Strategic Alliance (G0902418 and MC_UU_12025).

AUTHOR CONTRIBUTIONS

The project was conceived and supervised by A.N.B. Experiments were performed by K.T., S.E.J., and J.B. Reagents were generated by K.T., S.E.J., M.-A.D., and M.F. Mass spectrometry data were contributed by I.V., R.F., and B.M.K. J.R.C. supervised M.-A.D. The paper was written by A.N.B. with contributions from K.T. All authors agree that the contributions of K.T. and S.E.J. are equal and that their positions on the author list can be swapped around on CVs, websites, and elsewhere if desired.

DECLARATION OF INTERESTS

The authors declare no competing interests.

Received: March 18, 2023
Revised: October 10, 2023
Accepted: December 22, 2023
Published: January 23, 2024

REFERENCES

1. Blackford, A.N., and Jackson, S.P. (2017). ATM, ATR, and DNA-PK: The Trinity at the Heart of the DNA Damage Response. Mol. Cell *66*, 801–817.
2. Chen, C.C., Feng, W., Lim, P.X., Kass, E.M., and Jasin, M. (2018). Homology-Directed Repair and the Role of BRCA1, BRCA2, and Related Proteins in Genome Integrity and Cancer. Annu. Rev. Cancer Biol. *2*, 313–336.
3. Renkawitz, J., Lademann, C.A., and Jentsch, S. (2014). Mechanisms and principles of homology search during recombination. Nat. Rev. Mol. Cell Biol. *15*, 369–383.
4. Verma, P., and Greenberg, R.A. (2016). Noncanonical views of homology-directed DNA repair. Genes Dev. *30*, 1138–1154.
5. West, S.C., Blanco, M.G., Chan, Y.W., Matos, J., Sarbajna, S., and Wyatt, H.D.M. (2015). Resolution of Recombination Intermediates: Mechanisms and Regulation. Cold Spring Harb. Symp. Quant. Biol. *80*, 103–109.
6. Bythell-Douglas, R., and Deans, A.J. (2021). A Structural Guide to the Bloom Syndrome Complex. Structure *29*, 99–113.
7. Wu, L., and Hickson, I.D. (2003). The Bloom's syndrome helicase suppresses crossing over during homologous recombination. Nature *426*, 870–874.
8. Ellis, N.A., Groden, J., Ye, T.Z., Straughen, J., Lennon, D.J., Ciocci, S., Proytcheva, M., and German, J. (1995). The Bloom's syndrome gene product is homologous to RecQ helicases. Cell *83*, 655–666.
9. Hudson, D.F., Amor, D.J., Boys, A., Butler, K., Williams, L., Zhang, T., and Kalitsis, P. (2016). Loss of RMI2 Increases Genome Instability and Causes a Bloom-Like Syndrome. PLoS Genet. *12*, e1006483.
10. Martin, C.-A., Sarlós, K., Logan, C.V., Thakur, R.S., Parry, D.A., Bizard, A.H., Leitch, A., Cleal, L., Ali, N.S., Al-Owain, M.A., et al. (2018). Mutations in TOP3A Cause a Bloom Syndrome-like Disorder. Am. J. Hum. Genet. *103*, 221–231.
11. Gravel, S., Chapman, J.R., Magill, C., and Jackson, S.P. (2008). DNA helicases Sgs1 and BLM promote DNA double-strand break resection. Genes Dev. *22*, 2767–2772.
12. Nimonkar, A.V., Genschel, J., Kinoshita, E., Polaczek, P., Campbell, J.L., Wyman, C., Modrich, P., and Kowalczykowski, S.C. (2011). BLM-DNA2-RPA-MRN and EXO1-BLM-RPA-MRN constitute two DNA end resection machineries for human DNA break repair. Genes Dev. *25*, 350–362.
13. Sturzenegger, A., Burdová, K., Kanagaraj, R., Levikova, M., Pinto, C., Cejka, P., and Janscak, P. (2014). DNA2 Cooperates with the WRN and BLM RecQ Helicases to Mediate Long-range DNA End Resection in Human Cells. J. Biol. Chem. *289*, 27314–27326.
14. Chan, K.L., North, P.S., and Hickson, I.D. (2007). BLM is required for faithful chromosome segregation and its localization defines a class of ultrafine anaphase bridges. EMBO J. *26*, 3397–3409.
15. Ke, Y., Huh, J.W., Warrington, R., Li, B., Wu, N., Leng, M., Zhang, J., Ball, H.L., Li, B., and Yu, H. (2011). PICH and BLM limit histone association with anaphase centromeric DNA threads and promote their resolution. EMBO J. *30*, 3309–3321.
16. Davies, S.L., North, P.S., and Hickson, I.D. (2007). Role for BLM in replication-fork restart and suppression of origin firing after replicative stress. Nat. Struct. Mol. Biol. *14*, 677–679.
17. Shorrocks, A.-M.K., Jones, S.E., Tsukada, K., Morrow, C.A., Belblidia, Z., Shen, J., Vendrell, I., Fischer, R., Kessler, B.M., and Blackford, A.N. (2021). The Bloom syndrome complex senses RPA-coated single-stranded DNA to restart stalled replication forks. Nat. Commun. *12*, 585.
18. Ip, S.C.Y., Rass, U., Blanco, M.G., Flynn, H.R., Skehel, J.M., and West, S.C. (2008). Identification of Holliday junction resolvases from humans and yeast. Nature *456*, 357–361.
19. Andersen, S.L., Bergstralh, D.T., Kohl, K.P., LaRocque, J.R., Moore, C.B., and Sekelsky, J. (2009). Drosophila MUS312 and the vertebrate ortholog BTBD12 interact with DNA structure-specific endonucleases in DNA repair and recombination. Mol. Cell *35*, 128–135.
20. Fekairi, S., Scaglione, S., Chahwan, C., Taylor, E.R., Tissier, A., Coulon, S., Dong, M.Q., Ruse, C., Yates, J.R., Russell, P., et al. (2009). Human SLX4 is a Holliday junction resolvase subunit that binds multiple DNA repair/recombination endonucleases. Cell *138*, 78–89.
21. Muñoz, I.M., Hain, K., Déclais, A.C., Gardiner, M., Toh, G.W., Sanchez-Pulido, L., Heuckmann, J.M., Toth, R., Macartney, T., Eppink, B., et al. (2009). Coordination of structure-specific nucleases by human SLX4/BTBD12 is required for DNA repair. Mol. Cell *35*, 116–127.
22. Svendsen, J.M., Smogorzewska, A., Sowa, M.E., O'Connell, B.C., Gygi, S.P., Elledge, S.J., and Harper, J.W. (2009). Mammalian BTBD12/SLX4 assembles a Holliday junction resolvase and is required for DNA repair. Cell *138*, 63–77.
23. Wechsler, T., Newman, S., and West, S.C. (2011). Aberrant chromosome morphology in human cells defective for Holliday junction resolution. Nature *471*, 642–646.
24. Castor, D., Nair, N., Déclais, A.C., Lachaud, C., Toth, R., Macartney, T.J., Lilley, D.M.J., Arthur, J.S.C., and Rouse, J. (2013). Cooperative Control of Holliday Junction Resolution and DNA Repair by the SLX1 and MUS81-EME1 Nucleases. Mol. Cell *52*, 221–233.
25. Garner, E., Kim, Y., Lach, F.P., Kottemann, M.C., and Smogorzewska, A. (2013). Human GEN1 and the SLX4-Associated Nucleases MUS81 and SLX1 Are Essential for the Resolution of Replication-Induced Holliday Junctions. Cell Rep. *5*, 207–215.
26. Wyatt, H.D.M., Sarbajna, S., Matos, J., and West, S.C. (2013). Coordinated actions of SLX1-SLX4 and MUS81-EME1 for Holliday junction resolution in human cells. Mol. Cell *52*, 234–247.
27. Wyatt, H.D.M., Laister, R.C., Martin, S.R., Arrowsmith, C.H., and West, S.C. (2017). The SMX DNA Repair Tri-nuclease. Mol. Cell *65*, 848–860.e11.
28. Semlow, D.R., and Walter, J.C. (2021). Mechanisms of Vertebrate DNA Interstrand Cross-Link Repair. Annu. Rev. Biochem. *90*, 107–135.
29. Kim, Y., Lach, F.P., Desetty, R., Hanenberg, H., Auerbach, A.D., and Smogorzewska, A. (2011). Mutations of the SLX4 gene in Fanconi anemia. Nat. Genet. *43*, 142–146.
30. Stoepker, C., Hain, K., Schuster, B., Hilhorst-Hofstee, Y., Rooimans, M.A., Steltenpool, J., Oostra, A.B., Eirich, K., Korthof, E.T., Nieuwint, A.W.M., et al. (2011). SLX4, a coordinator of structure-specific endonucleases, is mutated in a new Fanconi anemia subtype. Nat. Genet. *43*, 138–141.
31. Bogliolo, M., Schuster, B., Stoepker, C., Derkunt, B., Su, Y., Raams, A., Trujillo, J.P., Minguillón, J., Ramírez, M.J., Pujol, R., et al. (2013). Mutations in ERCC4, encoding the DNA-repair endonuclease XPF, cause Fanconi anemia. Am. J. Hum. Genet. *92*, 800–806.
32. Kashiyama, K., Nakazawa, Y., Pilz, D.T., Guo, C., Shimada, M., Sasaki, K., Fawcett, H., Wing, J.F., Lewin, S.O., Carr, L., et al. (2013). Malfunction of nuclease ERCC1-XPF results in diverse clinical manifestations and causes Cockayne syndrome, xeroderma pigmentosum, and Fanconi anemia. Am. J. Hum. Genet. *92*, 807–819.
33. Yamamoto, K.N., Kobayashi, S., Tsuda, M., Kurumizaka, H., Takata, M., Kono, K., Jiricny, J., Takeda, S., and Hirota, K. (2011). Involvement of SLX4 in interstrand cross-link repair is regulated by the Fanconi anemia pathway. Proc. Natl. Acad. Sci. USA *108*, 6492–6496.
34. Klein Douwel, D., Boonen, R.A.C.M., Long, D.T., Szypowska, A.A., Räschle, M., Walter, J.C., and Knipscheer, P. (2014). XPF-ERCC1 Acts in Unhooking DNA Interstrand Crosslinks in Cooperation with FANCD2 and FANCP/SLX4. Mol. Cell *54*, 460–471.

35. Lachaud, C., Castor, D., Hain, K., Muñoz, I., Wilson, J., Macartney, T.J., Schindler, D., and Rouse, J. (2014). Distinct functional roles for the two SLX4 ubiquitin-binding UBZ domains mutated in Fanconi anemia. J. Cell Sci. *127*, 2811–2817.

36. Katsuki, Y., Abe, M., Park, S.Y., Wu, W., Yabe, H., Yabe, M., Attikum, H. van, Nakada, S., Ohta, T., Seidman, M.M., et al. (2021). RNF168 E3 ligase participates in ubiquitin signaling and recruitment of SLX4 during DNA crosslink repair. Cell Rep. *37*, 109879.

37. Sarbajna, S., Davies, D., and West, S.C. (2014). Roles of SLX1-SLX4, MUS81-EME1, and GEN1 in avoiding genome instability and mitotic catastrophe. Genes Dev. *28*, 1124–1136.

38. Boddy, M.N., Lopez-Girona, A., Shanahan, P., Interthal, H., Heyer, W.D., and Russell, P. (2000). Damage tolerance protein Mus81 associates with the FHA1 domain of checkpoint kinase Cds1. Mol. Cell. Biol. *20*, 8758–8766.

39. Mullen, J.R., Kaliraman, V., Ibrahim, S.S., and Brill, S.J. (2001). Requirement for three novel protein complexes in the absence of the Sgs1 DNA helicase in Saccharomyces cerevisiae. Genetics *157*, 103–118.

40. Johnson-Schlitz, D., and Engels, W.R. (2006). Template disruptions and failure of double Holliday junction dissolution during double-strand break repair in Drosophila BLM mutants. Proc. Natl. Acad. Sci. USA *103*, 16840–16845.

41. Andersen, S.L., Kuo, H.K., Savukoski, D., Brodsky, M.H., and Sekelsky, J. (2011). Three structure-selective endonucleases are essential in the absence of BLM helicase in Drosophila. PLoS Genet. *7*, e1002315.

42. Saito, T.T., Youds, J.L., Boulton, S.J., and Colaiácovo, M.P. (2009). Caenorhabditis elegans HIM-18/SLX-4 Interacts with SLX-1 and XPF-1 and Maintains Genomic Integrity in the Germline by Processing Recombination Intermediates. PLoS Genet. *5*, e1000735.

43. Bizard, A.H., and Hickson, I.D. (2014). The dissolution of double Holliday junctions. Cold Spring Harb. Perspect. Biol. *6*, a016477.

44. Tomimatsu, N., Mukherjee, B., Deland, K., Kurimasa, A., Bolderson, E., Khanna, K.K., and Burma, S. (2012). Exo1 plays a major role in DNA end resection in humans and influences double-strand break repair and damage signaling decisions. DNA Repair *11*, 441–448.

45. Cohen, S., Guenolé, A., Lazar, I., Marnef, A., Clouaire, T., Vernekar, D.V., Puget, N., Rocher, V., Arnould, C., Aguirrebengoa, M., et al. (2022). A POLD3/BLM dependent pathway handles DSBs in transcribed chromatin upon excessive RNA:DNA hybrid accumulation. Nat. Commun. *13*, 2012.

46. Xue, C., Salunkhe, S.J., Tomimatsu, N., Kawale, A.S., Kwon, Y., Burma, S., Sung, P., and Greene, E.C. (2022). Bloom helicase mediates formation of large single-stranded DNA loops during DNA end processing. Nat. Commun. *13*, 2248.

47. Ghamrasni, S.E., Cardoso, R., Halaby, M.J., Zeegers, D., Harding, S., Kumareswaran, R., Yavorska, T., Chami, N., Jurisicova, A., Sanchez, O., et al. (2014). Cooperation of Blm and Mus81 in development, fertility, genomic integrity and cancer suppression. Oncogene *34*, 1780–1789.

48. Patel, D.S., Misenko, S.M., Her, J., and Bunting, S.F. (2017). BLM helicase regulates DNA repair by counteracting RAD51 loading at DNA double-strand break sites. J. Cell Biol. *216*, 3521–3534.

49. Prakash, R., Sandoval, T., Morati, F., Zagelbaum, J.A., Lim, P.X., White, T., Taylor, B., Wang, R., Desclos, E.C.B., Sullivan, M.R., et al. (2021). Distinct pathways of homologous recombination controlled by the SWS1–SWSAP1–SPIDR complex. Nat. Commun. *12*, 4255.

50. Wu, L., Davies, S.L., Levitt, N.C., and Hickson, I.D. (2001). Potential role for the BLM helicase in recombinational repair via a conserved interaction with RAD51. J. Biol. Chem. *276*, 19375–19381.

51. Tripathi, V., Kaur, S., and SenGupta, S. (2008). Phosphorylation-dependent interactions of BLM and 53BP1 are required for their anti-recombinogenic roles during homologous recombination. Carcinogenesis *29*, 52–61.

52. Hu, Y., Raynard, S., Sehorn, M.G., Lu, X., Bussen, W., Zheng, L., Stark, J.M., Barnes, E.L., Chi, P., Janscak, P., et al. (2007). RECQL5/Recql5 helicase regulates homologous recombination and suppresses tumor formation via disruption of Rad51 presynaptic filaments. Genes Dev. *21*, 3073–3084.

53. Hosono, Y., Abe, T., Ishiai, M., Islam, M.N., Arakawa, H., Wang, W., Takeda, S., Ishii, Y., Takata, M., Seki, M., et al. (2014). Tumor suppressor RecQL5 controls recombination induced by DNA crosslinking agents. Biochim. Biophys. Acta *1843*, 1002–1012.

54. Paliwal, S., Kanagaraj, R., Sturzenegger, A., Burdová, K., and Janscak, P. (2014). Human RECQ5 helicase promotes repair of DNA double-strand breaks by synthesis-dependent strand annealing. Nucleic Acids Res. *42*, 2380–2390.

55. Ochs, F., Somyajit, K., Altmeyer, M., Rask, M.B., Lukas, J., and Lukas, C. (2016). 53BP1 fosters fidelity of homology-directed DNA repair. Nat. Struct. Mol. Biol. *23*, 714–721.

56. Bhattacharyya, A., Ear, U.S., Koller, B.H., Weichselbaum, R.R., and Bishop, D.K. (2000). The breast cancer susceptibility gene BRCA1 is required for subnuclear assembly of Rad51 and survival following treatment with the DNA cross-linking agent cisplatin. J. Biol. Chem. *275*, 23899–23903.

57. Wu, L.C., Wang, Z.W., Tsan, J.T., Spillman, M.A., Phung, A., Xu, X.L., Yang, M.C., Hwang, L.Y., Bowcock, A.M., and Baer, R. (1996). Identification of a RING protein that can interact in vivo with the BRCA1 gene product. Nat. Genet. *14*, 430–440.

58. Joukov, V., Chen, J., Fox, E.A., Green, J.B., and Livingston, D.M. (2001). Functional communication between endogenous BRCA1 and its partner, BARD1, during Xenopus laevis development. Proc. Natl. Acad. Sci. USA *98*, 12078–12083.

59. Moynahan, M.E., Chiu, J.W., Koller, B.H., and Jasin, M. (1999). Brca1 controls homology-directed DNA repair. Mol. Cell *4*, 511–518.

60. Yuan, S.S., Lee, S.Y., Chen, G., Song, M., Tomlinson, G.E., and Lee, E.Y. (1999). BRCA2 is required for ionizing radiation-induced assembly of Rad51 complex in vivo. Cancer Res. *59*, 3547–3551.

61. Moynahan, M.E., Pierce, A.J., and Jasin, M. (2001). BRCA2 is required for homology-directed repair of chromosomal breaks. Mol. Cell *7*, 263–272.

62. Adam, S., Rossi, S.E., Moatti, N., De Marco Zompit, M.D.M., Xue, Y., Ng, T.F., Álvarez-Quilón, A., Desjardins, J., Bhaskaran, V., Martino, G., et al. (2021). The CIP2A–TOPBP1 axis safeguards chromosome stability and is a synthetic lethal target for BRCA-mutated cancer. Nat. Cancer *2*, 1357–1371.

63. Shi, Y. (2004). Caspase Activation Revisiting the Induced Proximity Model. Cell *117*, 855–858.

64. Thomson, E.J., and Perry, P.E. (1988). The identification of micronucleated chromosomes: a possible assay for aneuploidy. Mutagenesis *3*, 415–418.

65. Bussen, W., Raynard, S., Busygina, V., Singh, A.K., and Sung, P. (2007). Holliday Junction Processing Activity of the BLM-Topo IIIα-BLAP75 Complex. J. Biol. Chem. *282*, 31484–31492.

66. Hodson, C., Low, J.K.K., Twest, S. van, Jones, S.E., Swuec, P., Murphy, V., Tsukada, K., Fawkes, M., Bythell-Douglas, R., Davies, A., et al. (2022). Mechanism of Bloom syndrome complex assembly required for double Holliday junction dissolution and genome stability. Proc. Natl. Acad. Sci. USA *119*, e2109093119.

67. Ceccaldi, R., Liu, J.C., Amunugama, R., Hajdu, I., Primack, B., Petalcorin, M.I.R., O'Connor, K.W., Konstantinopoulos, P.A., Elledge, S.J., Boulton, S.J., et al. (2015). Homologous-recombination-deficient tumours are dependent on Polθ-mediated repair. Nature *518*, 258–262.

68. Li, W., and Wang, J.C. (1998). Mammalian DNA topoisomerase IIIalpha is essential in early embryogenesis. Proc. Natl. Acad. Sci. USA *95*, 1010–1013.

69. Seki, M., Nakagawa, T., Seki, T., Kato, G., Tada, S., Takahashi, Y., Yoshimura, A., Kobayashi, T., Aoki, A., Otsuki, M., et al. (2006). Bloom

helicase and DNA topoisomerase IIIalpha are involved in the dissolution of sister chromatids. Mol. Cell. Biol. *26*, 6299–6307.

70. Mönnich, M., Hess, I., Wiest, W., Bachrati, C., Hickson, I.D., Schorpp, M., and Boehm, T. (2010). Developing T lymphocytes are uniquely sensitive to a lack of topoisomerase III alpha. Eur. J. Immunol. *40*, 2379–2384.
71. Chaganti, R.S., Schonberg, S., and German, J. (1974). A manyfold increase in sister chromatid exchanges in Bloom's syndrome lymphocytes. Proc. Natl. Acad. Sci. USA *71*, 4508–4512.
72. Zheng, L., Meng, Y., Campbell, J.L., and Shen, B. (2020). Multiple roles of DNA2 nuclease/helicase in DNA metabolism, genome stability and human diseases. Nucleic Acids Res. *48*, 16–35.
73. Sertic, S., Quadri, R., Lazzaro, F., and Muzi-Falconi, M. (2020). EXO1: A tightly regulated nuclease. DNA Repair *93*, 102929.
74. van de Kooij, B., Schreuder, A., Pavani, R.S., Garzero, V., Van Hoeck, A., San Martin Alonso, M., Koerse, D., Wendel, T.J., Callen, E., Boom, J., et al. (2024). EXO1-mediated DNA repair by single-strand annealing is essential for BRCA1-deficient cells. Mol. Cell *84*. https://doi.org/10.1016/j.molcel.2023.12.039.
75. Przetocka, S., Porro, A., Bolck, H.A., Walker, C., Lezaja, A., Trenner, A., Aesch, C. von, Himmels, S.F., D'Andrea, A.D., Ceccaldi, R., et al. (2018). CtIP-Mediated Fork Protection Synergizes with BRCA1 to Suppress Genomic Instability upon DNA Replication Stress. Mol. Cell *72*, 568–582.e6.
76. Bolck, H.A., Przetocka, S., Meier, R., Aesch, C. von, Zurfluh, C., Hänggi, K., Spegg, V., Altmeyer, M., Stebler, M., Nørrelykke, S.F., et al. (2022). RNAi Screening Uncovers a Synthetic Sick Interaction between CtIP and the BARD1 Tumor Suppressor. Cells *11*, 643.
77. Groelly, F.J., Fawkes, M., Dagg, R.A., Blackford, A.N., and Tarsounas, M. (2023). Targeting DNA damage response pathways in cancer. Nat. Rev. Cancer *23*, 78–94.
78. Zhang, F., Ma, J., Wu, J., Ye, L., Cai, H., Xia, B., and Yu, X. (2009). PALB2 links BRCA1 and BRCA2 in the DNA-damage response. Curr. Biol. *19*, 524–529.
79. Sy, S.M.H., Huen, M.S.Y., and Chen, J. (2009). PALB2 is an integral component of the BRCA complex required for homologous recombination repair. Proc. Natl. Acad. Sci. USA *106*, 7155–7160.
80. Zhang, F., Fan, Q., Ren, K., and Andreassen, P.R. (2009). PALB2 functionally connects the breast cancer susceptibility proteins BRCA1 and BRCA2. Mol. Cancer Res. *7*, 1110–1118.
81. Wong, A.K., Ormonde, P.A., Pero, R., Chen, Y., Lian, L., Salada, G., Berry, S., Lawrence, Q., Dayananth, P., Ha, P., et al. (1998). Characterization of a carboxy-terminal BRCA1 interacting protein. Oncogene *17*, 2279–2285.
82. Yu, X., Wu, L.C., Bowcock, A.M., Aronheim, A., and Baer, R. (1998). The C-terminal (BRCT) domains of BRCA1 interact in vivo with CtIP, a protein implicated in the CtBP pathway of transcriptional repression. J. Biol. Chem. *273*, 25388–25392.
83. Cantor, S.B., Bell, D.W., Ganesan, S., Kass, E.M., Drapkin, R., Grossman, S., Wahrer, D.C., Sgroi, D.C., Lane, W.S., Haber, D.A., et al. (2001). BACH1, a novel helicase-like protein, interacts directly with BRCA1 and contributes to its DNA repair function. Cell *105*, 149–160.
84. Wang, B., Matsuoka, S., Ballif, B.A., Zhang, D., Smogorzewska, A., Gygi, S.P., and Elledge, S.J. (2007). Abraxas and RAP80 form a BRCA1 protein complex required for the DNA damage response. Science *316*, 1194–1198.
85. Botuyan, M.V.E., Nominé, Y., Yu, X., Juranic, N., Macura, S., Chen, J., and Mer, G. (2004). Structural basis of BACH1 phosphopeptide recognition by BRCA1 tandem BRCT domains. Structure *12*, 1137–1146.
86. Clapperton, J.A., Manke, I.A., Lowery, D.M., Ho, T., Haire, L.F., Yaffe, M.B., and Smerdon, S.J. (2004). Structure and mechanism of BRCA1 BRCT domain recognition of phosphorylated BACH1 with implications for cancer. Nat. Struct. Mol. Biol. *11*, 512–518.
87. Williams, R.S., Lee, M.S., Hau, D.D., and Glover, J.N.M. (2004). Structural basis of phosphopeptide recognition by the BRCT domain of BRCA1. Nat. Struct. Mol. Biol. *11*, 519–525.
88. Zhao, W., Steinfeld, J.B., Liang, F., Chen, X., Maranon, D.G., Jian Ma, C.J., Kwon, Y., Rao, T., Wang, W., Sheng, C., et al. (2017). BRCA1-BARD1 promotes RAD51-mediated homologous DNA pairing. Nature *550*, 360–365.
89. Densham, R.M., Garvin, A.J., Stone, H.R., Strachan, J., Baldock, R.A., Daza-Martin, M., Fletcher, A., Blair-Reid, S., Beesley, J., Johal, B., et al. (2016). Human BRCA1-BARD1 ubiquitin ligase activity counteracts chromatin barriers to DNA resection. Nat. Struct. Mol. Biol. *23*, 647–655.
90. Reid, L.J., Shakya, R., Modi, A.P., Lokshin, M., Cheng, J.T., Jasin, M., Baer, R., and Ludwig, T. (2008). E3 ligase activity of BRCA1 is not essential for mammalian cell viability or homology-directed repair of double-strand DNA breaks. Proc. Natl. Acad. Sci. USA *105*, 20876–20881.
91. Shakya, R., Reid, L.J., Reczek, C.R., Cole, F., Egli, D., Lin, C.S., deRooij, D.G., Hirsch, S., Ravi, K., Hicks, J.B., et al. (2011). BRCA1 tumor suppression depends on BRCT phosphoprotein binding, but not its E3 ligase activity. Science *334*, 525–528.
92. Nakamura, K., Saredi, G., Becker, J.R., Foster, B.M., Nguyen, N.V., Beyer, T.E., Cesa, L.C., Faull, P.A., Lukauskas, S., Frimurer, T., et al. (2019). H4K20me0 recognition by BRCA1-BARD1 directs homologous recombination to sister chromatids. Nat. Cell Biol. *21*, 311–318.
93. Krais, J.J., Wang, Y., Patel, P., Basu, J., Bernhardy, A.J., and Johnson, N. (2021). RNF168-mediated localization of BARD1 recruits the BRCA1-PALB2 complex to DNA damage. Nat. Commun. *12*, 5016.
94. Laufer, M., Nandula, S.V., Modi, A.P., Wang, S., Jasin, M., Murty, V.V.V.S., Ludwig, T., and Baer, R. (2007). Structural requirements for the BARD1 tumor suppressor in chromosomal stability and homology-directed DNA repair. J. Biol. Chem. *282*, 34325–34333.
95. Becker, J.R., Clifford, G., Bonnet, C., Groth, A., Wilson, M.D., and Chapman, J.R. (2021). BARD1 reads H2A lysine 15 ubiquitination to direct homologous recombination. Nature *596*, 433–437.
96. Billing, D., Horiguchi, M., Wu-Baer, F., Taglialatela, A., Leuzzi, G., Nanez, S.A., Jiang, W., Zha, S., Szabolcs, M., Lin, C.S., et al. (2018). The BRCT Domains of the BRCA1 and BARD1 Tumor Suppressors Differentially Regulate Homology-Directed Repair and Stalled Fork Protection. Mol. Cell *72*, 127–139.e8.
97. Choudhury, A.D., Xu, H., Modi, A.P., Zhang, W., Ludwig, T., and Baer, R. (2005). Hyperphosphorylation of the BARD1 tumor suppressor in mitotic cells. J. Biol. Chem. *280*, 24669–24679.
98. Hayami, R., Sato, K., Wu, W., Nishikawa, T., Hiroi, J., Ohtani-Kaneko, R., Fukuda, M., and Ohta, T. (2005). Down-regulation of BRCA1-BARD1 Ubiquitin Ligase by CDK2. Cancer Res. *65*, 6–10.
99. Jumper, J., Evans, R., Pritzel, A., Green, T., Figurnov, M., Ronneberger, O., Tunyasuvunakool, K., Bates, R., Žídek, A., Potapenko, A., et al. (2021). Highly accurate protein structure prediction with AlphaFold. Nature *596*, 583–589.
100. Varadi, M., Anyango, S., Deshpande, M., Nair, S., Natassia, C., Yordanova, G., Yuan, D., Stroe, O., Wood, G., Laydon, A., et al. (2022). AlphaFold Protein Structure Database: massively expanding the structural coverage of protein-sequence space with high-accuracy models. Nucleic Acids Res. *50*, D439–D444.
101. Xu, Y., Ning, S., Wei, Z., Xu, R., Xu, X., Xing, M., Guo, R., and Xu, D. (2017). 53BP1 and BRCA1 control pathway choice for stalled replication restart. eLife *6*, 35897.
102. Gupta, R., Somyajit, K., Narita, T., Maskey, E., Stanlie, A., Kremer, M., Typas, D., Lammers, M., Mailand, N., Nussenzweig, A., et al. (2018). DNA Repair Network Analysis Reveals Shieldin as a Key Regulator of NHEJ and PARP Inhibitor Sensitivity. Cell *173*, 972–988.e23.
103. Xu, X., Xu, Y., Guo, R., Xu, R., Fu, C., Xing, M., Sasanuma, H., Li, Q., Takata, M., Takeda, S., et al. (2021). Fanconi anemia proteins participate

in a break-induced-replication-like pathway to counter replication stress. Nat. Struct. Mol. Biol. *28*, 487–500.

104. Alghoul, E., Paloni, M., Takedachi, A., Urbach, S., Barducci, A., Gaillard, P.H., Basbous, J., and Constantinou, A. (2023). Compartmentalization of the SUMO/RNF4 pathway by SLX4 drives DNA repair. Mol. Cell *83*, 1640–1658.e9.
105. Aprosoff, C.M., Dyakov, B.J.A., Cheung, V.H.W., Wong, C.J., Palandra, M., Gingras, A.C., and Wyatt, H.D.M. (2023). Comprehensive Interactome Mapping of the DNA Repair Scaffold SLX4 Using Proximity Labeling and Affinity Purification. J. Proteome Res. *22*, 1660–1681.
106. Payliss, B.J., Patel, A., Sheppard, A.C., and Wyatt, H.D.M. (2021). Exploring the Structures and Functions of Macromolecular SLX4-Nuclease Complexes in Genome Stability. Front. Genet. *12*, 784167.
107. Matos, J., Blanco, M.G., Maslen, S., Skehel, J.M., and West, S.C. (2011). Regulatory Control of the Resolution of DNA Recombination Intermediates during Meiosis and Mitosis. Cell *147*, 158–172.
108. Duda, H., Arter, M., Gloggnitzer, J., Teloni, F., Wild, P., Blanco, M.G., Altmeyer, M., and Matos, J. (2016). A Mechanism for Controlled Breakage of Under-replicated Chromosomes during Mitosis. Dev. Cell *39*, 740–755.
109. Payliss, B.J., Tse, Y.W.E., Reichheld, S.E., Lemak, A., Yun, H.Y., Houliston, S., Patel, A., Arrowsmith, C.H., Sharpe, S., and Wyatt, H.D.M. (2022). Phosphorylation of the DNA repair scaffold SLX4 drives folding of the SAP domain and activation of the MUS81-EME1 endonuclease. Cell Rep. *41*, 111537.
110. Barrows, J.K., Fullbright, G., and Long, D.T. (2021). BRCA1-BARD1 regulates transcription through BRD4 in Xenopus nucleoplasmic extract. Nucleic Acids Res. *49*, 3263–3273.
111. Crickard, J.B., Xue, C., Wang, W., Kwon, Y., Sung, P., and Greene, E.C. (2019). The RecQ helicase Sgs1 drives ATP-dependent disruption of Rad51 filaments. Nucleic Acids Res. *47*, 4694–4706.
112. Islam, M.N., Paquet, N., Fox, D., Dray, E., Zheng, X.F., Klein, H., Sung, P., and Wang, W. (2012). A Variant of the Breast Cancer Type 2 Susceptibility Protein (BRC) Repeat Is Essential for the RECQL5 Helicase to Interact with RAD51 Recombinase for Genome Stabilization. J. Biol. Chem. *287*, 23808–23818.
113. Ho, H.N., and West, S.C. (2022). Generation of double Holliday junction DNAs and their dissolution/resolution within a chromatin context. Proc. Natl. Acad. Sci. USA *119*, e2123420119.
114. Balbo Pogliano, C.B., Ceppi, I., Giovannini, S., Petroulaki, V., Palmer, N., Uliana, F., Gatti, M., Kasaciunaite, K., Freire, R., Seidel, R., et al. (2022). The CDK1-TOPBP1-PLK1 axis regulates the Bloom's syndrome helicase BLM to suppress crossover recombination in somatic cells. Sci. Adv. *8*, eabk0221.
115. Sarlós, K., Biebricher, A.S., Bizard, A.H., Bakx, J.A.M., Ferreté-Bonastre, A.G., Modesti, M., Paramasivam, M., Yao, Q., Peterman, E.J.G., Wuite, G.J.L., et al. (2018). Reconstitution of anaphase DNA bridge recognition and disjunction. Nat. Struct. Mol. Biol. *25*, 868–876.
116. Deng, L., Wu, R.A., Sonneville, R., Kochenova, O.V., Labib, K., Pellman, D., and Walter, J.C. (2019). Mitotic CDK Promotes Replisome Disassembly, Fork Breakage, and Complex DNA Rearrangements. Mol. Cell *73*, 915–929.e6.
117. Heijink, A.M., Stok, C., Porubsky, D., Manolika, E.M., Kanter, J.K. de, Kok, Y.P., Everts, M., Boer, H.R. de, Audrey, A., Bakker, F.J., et al. (2022). Sister chromatid exchanges induced by perturbed replication can form independently of BRCA1, BRCA2 and RAD51. Nat. Commun. *13*, 6722.
118. German, J., Archibald, R., and Bloom, D. (1965). Chromosomal Breakage in a Rare and Probably Genetically Determined Syndrome of Man. Science *148*, 506–507.
119. Bouwman, P., Aly, A., Escandell, J.M., Pieterse, M., Bartkova, J., van der Gulden, H.V.D., Hiddingh, S., Thanasoula, M., Kulkarni, A., Yang, Q., et al. (2010). 53BP1 loss rescues BRCA1 deficiency and is associated with triple-negative and BRCA-mutated breast cancers. Nat. Struct. Mol. Biol. *17*, 688–695.
120. Bunting, S.F., Callén, E., Wong, N., Chen, H.T., Polato, F., Gunn, A., Bothmer, A., Feldhahn, N., Fernandez-Capetillo, O., Cao, L., et al. (2010). 53BP1 inhibits homologous recombination in Brca1-deficient cells by blocking resection of DNA breaks. Cell *141*, 243–254.
121. Nguyen, G.H., Dexheimer, T.S., Rosenthal, A.S., Chu, W.K., Singh, D.K., Mosedale, G., Bachrati, C.Z., Schultz, L., Sakurai, M., Savitsky, P., et al. (2013). A Small Molecule Inhibitor of the BLM Helicase Modulates Chromosome Stability in Human Cells. Chem. Biol. *20*, 55–62.
122. Chen, X., Ali, Y.I., Fisher, C.E., Arribas-Bosacoma, R., Rajasekaran, M.B., Williams, G., Walker, S., Booth, J.R., Hudson, J.J., Roe, S.M., et al. (2021). Uncovering an allosteric mode of action for a selective inhibitor of human Bloom syndrome protein. eLife *10*, e65339.
123. Hastings, P.J., Ira, G., and Lupski, J.R. (2009). A Microhomology-Mediated Break-Induced Replication Model for the Origin of Human Copy Number Variation. PLoS Genet. *5*, e1000327.
124. Chan, Y.W., Fugger, K., and West, S.C. (2018). Unresolved recombination intermediates lead to ultra-fine anaphase bridges, chromosome breaks and aberrations. Nat. Cell Biol. *20*, 92–103.
125. Tacconi, E.M., Lai, X., Folio, C., Porru, M., Zonderland, G., Badie, S., Michl, J., Sechi, I., Rogier, M., Matía García, V.M., et al. (2017). BRCA1 and BRCA2 tumor suppressors protect against endogenous acetaldehyde toxicity. EMBO Mol. Med. *9*, 1398–1414.
126. Zimmer, J., Tacconi, E.M.C., Folio, C., Badie, S., Porru, M., Klare, K., Tumiati, M., Markkanen, E., Halder, S., Ryan, A., et al. (2016). Targeting BRCA1 and BRCA2 Deficiencies with G-Quadruplex-Interacting Compounds. Mol. Cell *61*, 449–460.
127. Chiang, T.-W.W., Sage, C. le, Larrieu, D., Demir, M., and Jackson, S.P. (2016). CRISPR-Cas9(D10A) nickase-based genotypic and phenotypic screening to enhance genome editing. Sci. Rep. *6*, 24356.
128. Dev, H., Chiang, T.-W.W., Lescale, C., Krijger, I. de, Martin, A.G., Pilger, D., Coates, J., Sczaniecka-Clift, M., Wei, W., Ostermaier, M., et al. (2018). Shieldin complex promotes DNA end-joining and counters homologous recombination in BRCA1-null cells. Nat. Cell Biol. *20*, 954–965.
129. Janicki, S.M., Tsukamoto, T., Salghetti, S.E., Tansey, W.P., Sachidanandam, R., Prasanth, K.V., Ried, T., Shav-Tal, Y., Bertrand, E., Singer, R.H., et al. (2004). From Silencing to Gene Expression Real-Time Analysis in Single Cells. Cell *116*, 683–698.
130. Schindelin, J., Arganda-Carreras, I., Frise, E., Kaynig, V., Longair, M., Pietzsch, T., Preibisch, S., Rueden, C., Saalfeld, S., Schmid, B., et al. (2012). Fiji: an open-source platform for biological-image analysis. Nature Methods *9*, 676–682.
131. Notredame, C., Higgins, D.G., and Heringa, J. (2000). T-Coffee: A novel method for fast and accurate multiple sequence alignment. J. Mol. Biol. *302*, 205–217.
132. Miles, A.J., Ramalli, S.G., and Wallace, B.A. (2022). DichroWeb, a website for calculating protein secondary structure from circular dichroism spectroscopic data. Protein Sci. *31*, 37–46.
133. Hannus, M., Beitzinger, M., Engelmann, J.C., Weickert, M.T., Spang, R., Hannus, S., and Meister, G. (2014). siPools: highly complex but accurately defined siRNA pools eliminate off-target effects. Nucleic Acids Res. *42*, 8049–8061.
134. Campeau, E., Ruhl, V.E., Rodier, F., Smith, C.L., Rahmberg, B.L., Fuss, J.O., Campisi, J., Yaswen, P., Cooper, P.K., and Kaufman, P.D. (2009). A versatile viral system for expression and depletion of proteins in mammalian cells. PLoS One *4*, e6529.
135. Dundr, M., Ospina, J.K., Sung, M.H., John, S., Upender, M., Ried, T., Hager, G.L., and Matera, A.G. (2007). Actin-dependent intranuclear repositioning of an active gene locus in vivo. J. Cell Biol. *179*, 1095–1103.
136. Orthwein, A., Noordermeer, S.M., Wilson, M.D., Landry, S., Enchev, R.I., Sherker, A., Munro, M., Pinder, J., Salsman, J., Dellaire, G., et al. (2015). A

mechanism for the suppression of homologous recombination in G1 cells. Nature *528*, 422–426.

137. Meerbrey, K.L., Hu, G., Kessler, J.D., Roarty, K., Li, M.Z., Fang, J.E., Herschkowitz, J.I., Burrows, A.E., Ciccia, A., Sun, T., et al. (2011). The pINDUCER lentiviral toolkit for inducible RNA interference in vitro and in vivo. Proc. Natl. Acad. Sci. USA *108*, 3665–3670.

138. Ran, F.A., Hsu, P.D., Wright, J., Agarwala, V., Scott, D.A., and Zhang, F. (2013). Genome engineering using the CRISPR-Cas9 system. Nat. Protoc. *8*, 2281–2308.

139. Hertzog, J., Dias Junior, A.G.D., Rigby, R.E., Donald, C.L., Mayer, A., Sezgin, E., Song, C., Jin, B., Hublitz, P., Eggeling, C., et al. (2018). Infection with a Brazilian isolate of Zika virus generates RIG-I stimulatory RNA and the viral NS5 protein blocks type I IFN induction and signaling. Eur. J. Immunol. *48*, 1120–1136.

140. Becker, J.R., Cuella-Martin, R., Barazas, M., Liu, R., Oliveira, C., Oliver, A.W., Bilham, K., Holt, A.B., Blackford, A.N., Heierhorst, J., et al. (2018). The ASCIZ-DYNLL1 axis promotes 53BP1-dependent non-homologous end joining and PARP inhibitor sensitivity. Nat. Commun. *9*, 5406.

141. Goldman, M.J., Craft, B., Hastie, M., Repečka, K., McDade, F., Kamath, A., Banerjee, A., Luo, Y., Rogers, D., Brooks, A.N., et al. (2020). Visualizing and interpreting cancer genomics data via the Xena platform. Nat. Biotechnol. *38*, 675–678.

142. Lees, J.G., Miles, A.J., Wien, F., and Wallace, B.A. (2006). A reference database for circular dichroism spectroscopy covering fold and secondary structure space. Bioinformatics *22*, 1955–1962.

143. Perez-Riverol, Y., Bai, J., Bandla, C., García-Seisdedos, D., Hewapathirana, S., Kamatchinathan, S., Kundu, D.J., Prakash, A., Frericks-Zipper, A., Eisenacher, M., et al. (2022). The PRIDE database resources in 2022: a hub for mass spectrometry-based proteomics evidences. Nucleic Acids Res. *50*, D543–D552.

CellPress
OPEN ACCESS

STAR★METHODS

KEY RESOURCES TABLE

REAGENT or RESOURCE	SOURCE	IDENTIFIER
Antibodies		
53BP1	Santa Cruz Biotechnology	sc-22760; RRID: AB_2256326
Abraxas	Abcam	ab139191; RRID: AB_2888912
BARD1	Abcam	ab64164; RRID: AB_1924804
BARD1	Bethyl Laboratories	A300-263A; RRID: AB_2061250
BLM	Bethyl Laboratories	A300-110A; RRID: AB_2064794
BRCA1	Santa Cruz Biotechnology	sc-6954; RRID: AB_626761
BRCA2	Merck	OP95; RRID: AB_2067762
Centromere (CREST)	Immunovision	HCT-0100; RRID: AB_2744669
CtIP	Abcam	ab155988
EME1	Santa Cruz Biotechnology	sc-53275; RRID: AB_2278026
ERCC1	Santa Cruz Biotechnology	sc-56673; RRID: AB_783261
EXO1	Abcam	ab95068; RRID: AB_10675762
FANCJ	Cell Signaling	4578; RRID: AB_2061832
GFP	Roche	11814460001; RRID: AB_390913
GST	Santa Cruz Biotechnology	sc-138; RRID: AB_627677
H2AX	Novus Biologicals	NB100-383; RRID: AB_10002060
H2AX-pS139	Millipore	05-636; RRID: AB_309864
KAP1	Abcam	ab10483; RRID: AB_297222
KAP1-pS824	Bethyl Laboratories	IHC-00073; RRID: AB_577234
MUS81	Santa Cruz Biotechnology	sc-53382; RRID: AB_2147138
PALB2	Bethyl Laboratories	A301-246A; RRID: AB_890607
PICH	Millipore	04-1540; RRID: AB_11210090
RAD51	BioAcademia	70-002; RRID: AB_1056187
RECQL5	Bethyl Laboratories	A302-520A; RRID: AB_1999022
RMI1	Novus Biologicals	NB100-1720; RRID: AB_2181500
RPA2	Abcam	ab10359; RRID: AB_297095
SLX1	Proteintech	21158-1-AP; RRID: AB_2752255
SLX4	Novus Biologicals	NBP1-28680; RRID: AB_2259342
SLX4IP	Santa Cruz Biotechnology	sc-377066; RRID: AB_2752253
TOP3A	Proteintech	14525-1-1AP; RRID: AB_2205881
XPF	Bethyl Laboratories	A301-315A; RRID: AB_938089
Donkey anti-rabbit IgG Alexa Fluor 568	Thermo Fisher Scientific	A10042; RRID: AB_2534017
Goat anti-mouse IgG Alexa Fluor Plus 488	Thermo Fisher Scientific	A32723; RRID: AB_2633275
Goat anti-mouse IgG1 Alexa Fluor 647	Thermo Fisher Scientific	A21240; RRID: AB_2535809
Cy3 AffiniPure Goat Anti-Human IgG	Jackson ImmunoResearch	109-165-003; RRID: AB_2337718
Bacterial and virus strains		
One Shot TOP10 Chemically Competent *E. coli*	Thermo Fisher Scientific	C404010
One Shot Stbl3 Chemically Competent *E. coli*	Thermo Fisher Scientific	C737303
Biological samples		
HeLa nuclear extract	Ipracell	CC-01-20-25
Chemicals, peptides, and recombinant proteins		
Aphidicolin	Santa Cruz Biotechnology	sc-201535

(*Continued on next page*)

Continued

REAGENT or RESOURCE	SOURCE	IDENTIFIER
BARD1 S148 peptide:Biotin-SGSG-KNSIKMWFSPRSKKVRYVVSK	Biomatik	N/A
BARD1 pS148 peptide:Biotin-SGSG-KNSIKMWF(pS)PRSKKVRYVVSK	Biomatik	N/A
BARD1 T299 peptide:Biotin-SGSG-TKSRNEVVTPEKVCKNYLTSK	Genosphere Technologies	N/A
BARD1 pT299 peptide:Biotin-SGSG-TKSRNEVV(pT)PEKVCKNYLTSK	Genosphere Technologies	N/A
BrdU	Thermo Fisher Scientific	H27260
Cisplatin	Merck	P4394
Colcemid	Merck	C9754
cOmplete EDTA-free Protease Inhibitor Cocktail	Merck	5056489001
DAPI	BD Biosciences	564907
Doxycycline	Merck	D9891
Dynabeads M-280	Thermo Fisher Scientific	11205D
GFP-Trap Magnetic Agarose	Proteintech	gtma
Giemsa Stain	Merck	48900
Hoechst	Merck	H6024
IAA	Merck	I2886
Lipofectamine 2000	Thermo Fisher Scientific	11668019
Lipofectamine 3000	Thermo Fisher Scientific	L3000015
Lipofectamine RNAiMAX	Thermo Fisher Scientific	13778150
Mowiol	Merck	81381
Nocodazole	Merck	487928
Olaparib	APExBIO	A4154
RAD17 peptide:Biotin-SGSG-LPLSQNSASELPASQPQPFS	Biomatik	N/A
RO-3306 (CDK1 inhibitor)	Merck	SML0569
SPOT-Trap Magnetic Agarose	Proteintech	etma
SuperNuclease	Sino Biological	SSNP01
VECTASHIELD Antifade Mounting Medium	Vector Laboratories	H-1000-10
Critical commercial assays		
BD Cytofix/Cytoperm Fixation and Permeabilization Solution	BD Biosciences	554722
Bolt 4%–12% Bis-Tris Plus Gels	Thermo Fisher Scientific	NW04120BOX
Caspase-Glo 3/7 Assay System	Promega	G8090
GenElute HP Endotoxin-Free Plasmid Maxiprep Kit	Merck	NA0410
Gateway BP Clonase II Enzyme mix	Thermo Fisher Scientific	11789020
Gateway LR Clonase II Enzyme mix	Thermo Fisher Scientific	11791020
Deposited data		
Mass spectrometry	This study	PRIDE: PXD042480
Raw western blots and imaging data	This study	Mendeley Data: https://doi.org/10.17632/yx7ym3rj6s.1
Experimental models: Cell lines		
293 Flp-In TREX	Steve West[124]	N/A
293 Flp-In TREX Δ*MUS81*	Steve West[124]	N/A
293 Flp-In TREX Δ*SLX1*	Steve West[124]	N/A
293FT	Thermo Fisher Scientific	R70007
H1299 shBRCA1	Madalena Tarsounas[125]	N/A
H1299 shBRCA2	Madalena Tarsounas[126]	N/A

(*Continued on next page*)

CellPress
OPEN ACCESS

Continued

REAGENT or RESOURCE	SOURCE	IDENTIFIER
HCT116 *BARD1*$^{AID/AID}$	Nakamura et al.[92]	N/A
HCT116 *BARD1*$^{AID/AID}$ +GST	Nakamura et al.[92]	N/A
HCT116 *BARD1*$^{AID/AID}$ +BARD1^{WT}	Nakamura et al.[92]	N/A
HCT116 *BARD1*$^{AID/AID}$ +BARD1^{R99E}	Nakamura et al.[92]	N/A
HCT116 *BARD1*$^{AID/AID}$ +BARD1^{S148A}	This paper	N/A
HCT116 *BARD1*$^{AID/AID}$ +BARD1^{ARD-3A}	Nakamura et al.[92]	N/A
HCT116 *BARD1*$^{AID/AID}$ +BARD1^{K619A}	Nakamura et al.[92]	N/A
HCT116 *BARD1*$^{AID/AID}$ +BARD1^{D712A}	Becker et al.[95]	N/A
HCT116 *BARD1*$^{AID/AID}$ +Spot-BARD1^{WT} +GFP-SLX4	This paper	N/A
HCT116 *BARD1*$^{AID/AID}$ Δ*BLM*	This paper	N/A
HCT116 *BARD1*$^{AID/AID}$ Δ*BLM* +GFP-SLX4	This paper	N/A
HCT116 *BARD1*$^{AID/AID}$ Δ*BLM* +Spot-BARD1^{WT}	This paper	N/A
HCT116 *BARD1*$^{AID/AID}$ Δ*BLM* +Spot-BARD1^{S148A}	This paper	N/A
HCT116 *BARD1*$^{AID/AID}$ Δ*BLM* +Spot-BARD1^{WT} +GFP-SLX4	This paper	N/A
HCT116 *BARD1*$^{AID/AID}$ Δ*BLM* +Spot-BARD1^{S148A} +GFP-SLX4	This paper	N/A
RPE1 FRT/TR Δ*TP53*	This paper	N/A
RPE1 FRT/TR Δ*TP53* +GFP	This paper	N/A
RPE1 FRT/TR Δ*TP53* Δ*BLM*	This paper	N/A
RPE1 FRT/TR Δ*TP53* Δ*BLM* +GFP	This paper	N/A
RPE1 FRT/TR Δ*TP53* Δ*BLM* +GFP-BLM^{WT}	This paper	N/A
RPE1 FRT/TR Δ*TP53* Δ*BLM* +GFP-BLM^{ΔTR}	This paper	N/A
RPE1 FRT/TR Δ*TP53* Δ*BLM* +GFP-BLM^{K695R}	This paper	N/A
RPE1 FRT/TR Δ*TP53* Δ*RECQL5*	This paper	N/A
RPE1 FRT/TR Δ*TP53*	Steve Jackson[127]	N/A
RPE1 FRT/TR Δ*TP53* Δ*BRCA1*	Steve Jackson[128]	N/A
RPE1 FRT/TR Δ*TP53* Δ*TP53BP1*	Steve Jackson[128]	N/A
RPE1 FRT/TR Δ*TP53* Δ*BRCA1* Δ*TP53BP1*	Steve Jackson[128]	N/A
RPE1 FRT/TR Δ*TP53* Δ*BRCA1* +GFP	This paper	N/A
RPE1 FRT/TR Δ*TP53* Δ*BRCA1* +GFP-BRCA1^{WT}	This paper	N/A
RPE1 FRT/TR Δ*TP53* Δ*BRCA1* +GFP-BRCA1^{ΔCC}	This paper	N/A
RPE1 FRT/TR Δ*TP53* Δ*BRCA1* +GFP-BRCA1^{S1655A}	This paper	N/A
U2OS 2-6-3	Roger Greenberg[129]	N/A
Oligonucleotides		
siCtrl:5′-CGUACGCGGAAUACUUCGA-3′	Eurofins Genomics	N/A
siBRCA1 #1 (pool)	siTOOLs Biotech	si-G050-672
siBRCA1 #2: 5′-CAGCUACCCUUCCAUCAUAUU-3	Eurofins Genomics	N/A
siBRCA2 (pool)	Horizon Discovery	L-003462-00-0005
siBLM #1:5′-GCUAGGAGUCUGCGUGCGA-3′	Eurofins Genomics	N/A
siBLM #2:5′-CUUUCUUGUUUGUCAGCAU-3′	Eurofins Genomics	N/A
siEXO1 (pool)	Horizon Discovery	L-013120-00-0005
siMUS81 (pool)	Horizon Discovery	L-016143-01-0005
siPICH (pool)	Horizon Discovery	L-031581-01-0005
siRMI1 #1:5′-AGCCUUCACGAAUGUUGAU-3′	Eurofins Genomics	N/A
siRMI1 #2:5′-GAUCCAGUAGGUAGGACAUUU-3′	Eurofins Genomics	N/A
siSLX4 (pool)	Horizon Discovery	L-014895-00-0005

(*Continued on next page*)

Continued

REAGENT or RESOURCE	SOURCE	IDENTIFIER
siTOP3A #1:5′-CCAGAAAUCUUCCACAGAA-3′	Eurofins Genomics	N/A
siTOP3A #2:5′-GCAGAGAUGUCUAAUGAAA-3′	Eurofins Genomics	N/A
si53BP1:5′-GCACACUUGUCACUCGUGU-3′	Thermo Fisher Scientific	s14314
sgRNA targeting RECQL5 #1 F:CACCGGACAACTTCAATGAAAAGGC	Thermo Fisher Scientific	N/A
sgRNA targeting RECQL5 #1 R:AAACGCCTTTTCATTGAAGTTGTCC	Thermo Fisher Scientific	N/A
sgRNA targeting RECQL5 #2 F:CACCGGCCCAAAAAGATTCGGGGA	Thermo Fisher Scientific	N/A
sgRNA targeting RECQL5 #2 R:AAACTCCCCGAATCTTTTTGGGCC	Thermo Fisher Scientific	N/A
BARD1 cloning primer F: AAGCTTGGTACCGAG CTCGGATCCATGCCAGACCGCGTGCGCGC	Thermo Fisher Scientific	N/A
BARD1 cloning primer R: CTGTGCTGGATATCT GCAGAATTCTCAGCTGTCAAGAGGAAGCA	Thermo Fisher Scientific	N/A
BARD1-S148A mutagenesis primer F: CTT TCTTACTTCGAGGGGCAAACCACAT TTTAATTGAATTCTTCTTGTTTCC	Thermo Fisher Scientific	N/A
BARD1-S148A mutagenesis primer R: GG AAACAAGAAGAATTCAATTAAAATGTGG TTTGCCCCTCGAAGTAAGAAAG	Thermo Fisher Scientific	N/A
GFP-SLX4 cloning primer F: GGTTCTAG AGCGCTGCCACCATGGTGAGCA AGGGCGAGGA	Thermo Fisher Scientific	N/A
GFP-SLX4 cloning primer R: CGCTCT GCCCGGATGCTAGCTCAGTTCC GCTCCACCTTCT	Thermo Fisher Scientific	N/A
Cherry-LacRep-BARD1 cloning primer F: AAGATCGAGTGGCATGAGGGATCCGG CAGCCCTAGATCTATGCC	Thermo Fisher Scientific	N/A
Cherry-LacRep-BARD1 cloning primer R: CAGTTATCTAGATCCGGTGGATCCTCAG CTGTCAAGAGGAAGCA	Thermo Fisher Scientific	N/A
BLM DTR mutagenesis primer F: GAT CGAGGGTAGAATGGCTGCTAAAA AGAAAACATCTTCAGATAA	Thermo Fisher Scientific	N/A
BLM DTR mutagenesis primer R: TTA TCTGAAGATGTTTTCTTTTTAGCAG CCATTCTACCCTCGATC	Thermo Fisher Scientific	N/A
BLM K695R mutagenesis primer F: GCCGACTGGAGGTGGTAGGA GTTTGTGTTACCAG	Thermo Fisher Scientific	N/A
BLM K695R mutagenesis primer R: CTGGTAACACAAACTCCTAC CACCTCCAGTCGGC	Thermo Fisher Scientific	N/A
BLM cloning primer F: GGGGACAAGT TTGTACAAAAAAGCAGGCTTCATG GTGAGCAAGGGCG	Thermo Fisher Scientific	N/A
BLM cloning primer R: GGGGACCACTT TGTACAAGAAAGCTGGGTTCATGA GAATGCATATGAAGGC	Thermo Fisher Scientific	N/A
BRCA1 S1655A mutagenesis primer F: CATGGTGGTGGCTGGCCTGACC	Thermo Fisher Scientific	N/A

(*Continued on next page*)

CellPress
OPEN ACCESS

Continued

REAGENT or RESOURCE	SOURCE	IDENTIFIER
BRCA1 S1655A mutagenesis primer R: GACATTCTTTTGTTGACC	Thermo Fisher Scientific	N/A
BRCA1 ΔCC mutagenesis primer F: TCTTCTGCCCTTGAGGAC	Thermo Fisher Scientific	N/A
BRCA1 ΔCC mutagenesis primer R: ACCTAAGTTTGAATCCATGC	Thermo Fisher Scientific	N/A
Recombinant DNA		
AIO-GFP-sgBLM	Shorrocks et al.[17]	N/A
PX458	Addgene	48138
PX458-GFP-RECQL5 targeting vector #1	This paper	N/A
PX458-mRuby2-RECQL5 targeting vector #2	This paper	N/A
pDONR221-GFP	Shorrocks et al.[17]	N/A
pLenti-PGK-Neo-DEST	Addgene	19067
pLenti-PGK-Neo-DEST-GFP	Shorrocks et al.[17]	N/A
pDONR221-GFP-BLM^{WT}	Hodson et al.[66]	N/A
pLenti-PGK-Neo-DEST-BLM^{WT}	Hodson et al.[66]	N/A
pDONR221-GFP-BLM$^{\Delta TR}$	This paper	N/A
pLenti-PGK-Neo-DEST-GFP-BLM$^{\Delta TR}$	This paper	N/A
pDONR221-GFP-BLM^{K695R}	Hodson et al.[66]	N/A
pLenti-PGK-Neo-DEST-GFP-BLM^{K695R}	Hodson et al.[66]	N/A
pDONR221-BARD1^{WT}	Nakamura et al.[92]	N/A
pDONR221-BARD1^{S148A}	This paper	N/A
pLenti-PGK-Neo-DEST-BARD1^{WT}	This paper	N/A
pLenti-PGK-Neo-DEST-BARD1^{S148A}	This paper	N/A
pDONR221-SPOT-BARD1^{WT}	This paper	N/A
pDONR221-SPOT-BARD1^{S148A}	This paper	N/A
pLenti-PGK-Neo-DEST-SPOT-BARD1^{WT}	This paper	N/A
pLenti-PGK-Neo-DEST-SPOT-BARD1^{S148A}	This paper	N/A
pcDNA3.1(+)	Thermo Fisher Scientific	V79020
pcDNA3.1-SPOT-BARD1^{WT}	This paper	N/A
pcDNA3.1-SPOT-BARD1^{S148A}	This paper	N/A
pcDNA5/FRT/TO-GFP-SLX4	John Rouse[21]	N/A
TLCV2-GFP-SLX4	This paper	N/A
Cherry-LacRep	Addgene	18985
Cherry-LacRep-BARD1^{WT}	This paper	N/A
Cherry-LacRep-BARD1^{S148A}	This paper	N/A
pInducer20	Addgene	44012
pInducer20-GFP	This paper	N/A
pDEST-FRT/TO-GFP-BRCA1	Addgene	71116
pInducer20-GFP-BRCA1^{WT}	This paper	N/A
pInducer20-GFP-BRCA1$^{\Delta CC}$	This paper	N/A
pInducer20-GFP-BRCA1^{S1655A}	This paper	N/A
Software and algorithms		
Fiji	Schindelin et al.[130]	https://imagej.net/software/fiji/
Prism 10	GraphPad	https://www.graphpad.com
scanR acquisition & analysis software	Olympus	https://www.olympus-lifescience.com/en/microscopes/inverted/scanr/

(*Continued on next page*)

Continued

REAGENT or RESOURCE	SOURCE	IDENTIFIER
LAS X	Leica Microsystems	https://www.leica-microsystems.com/products/microscope-software/p/leica-las-x-ls/
AlphaFold	Deepmind	https://alphafold.ebi.ac.uk
Spotfire	TIBCO	https://www.spotfire.com
pyBoxshade	M. Baron	https://github.com/mdbaron42/pyBoxshade
T-Coffee multiple sequence alignment tool	Notredame et al.[131]	https://www.ebi.ac.uk/Tools/msa/tcoffee/
DichroWeb	Miles et al.[132]	https://dichroweb.cryst.bbk.ac.uk/home.shtml
ZEN Black	ZEISS	https://www.micro-shop.zeiss.com/en/us/softwarefinder/software-categories/zen-black/

RESOURCE AVAILABILITY

Lead contact

Further information and requests for resources and reagents should be directed to and will be fulfilled by the lead contact, Andrew N. Blackford (andrew.blackford@imm.ox.ac.uk).

Materials availability

Unique reagents generated and described during this study are available on request.

Data and code availability

- Raw western blots and imaging data reported in this paper have been deposited at Mendeley and are publicly available as of the date of publication. The DOI is listed in the key resources table. Raw proteomics data have been deposited on PRIDE. The identifier is listed in the key resources table.
- This paper does not report original code.
- Any additional information required to reanalyze the data reported in this paper is available from the lead contact upon request.

EXPERIMENTAL MODEL AND STUDY PARTICIPANT DETAILS

Cell lines and culture conditions

All cells were grown in humidified incubators supplied with 5% CO_2 and maintained at 37 °C, with regular testing for mycoplasma contamination by LookOut Mycoplasma PCR Detection Kit (Merck). RPE-1 FRT/TR cells were purchased from Ximbio and cultured in Dulbecco's modified Eagle's medium (DMEM; Thermo Fisher Scientific) supplemented with 10% fetal calf serum (FCS; Thermo Fisher Scientific) and 100 u/ml penicillin/100 mg/ml streptomycin (Lonza). RPE-1 FRT/TR Δ*BLM* cell lines and their derivatives have been described previously.[17,66] Δ*BRCA1*, Δ*TP53BP1*, Δ*BRCA1*/Δ*TP53BP1* and their parental RPE-1 FRT/TR Δ*TP53* clones were gifts from Stephen Jackson.[127,128]

HCT116 *BARD1*$^{AID/AID}$ cell lines and their derivatives have been described previously.[92,95] H1299 cells expressing shRNAs targeting BRCA1 or BRCA2 were gifts from Madalena Tarsounas.[125,126] Δ*MUS81*, Δ*SLX1* and their parental 293 cells were gifts from Stephen West.[124] The U2OS 2-6-3 cell line containing an integrated array of ~256 *lacO* repeats was a gift from Roger Greenberg.[129] HCT116, H1299, 293 and U2OS cells were cultured in the same media as RPE-1 cells. 293FT cells were obtained from Thermo Fisher Scientific and cultured in DMEM supplemented with 10% FCS, 2 mM glutamine (Lonza), 1% MEM non-essential amino acids (Thermo Fisher Scientific) and 500 μg/ml Geneticin (G418; Thermo Fisher Scientific).

METHOD DETAILS

RNA interference

siRNAs were transfected using Lipofectamine RNAiMAX (Thermo Fisher Scientific) according to the manufacturer's instructions, with the following sequences: siCtrl (targeting firefly luciferase), 5'-CGUACGCGGAAUACUUCGA-3'; siBRCA1 #2, 5'-CAGCUACCCUUCCAUCAUAUU-3'; siBLM #1 5'-GCUAGGAGUCUGCGUGCGA-3'; siBLM #2, 5'-CUUUCUUGUUUGUCAGCAU-3'; siRMI1 #1, 5'-AGCCUUCACGAAUGUUGAU-3'; siRMI1 #2, 5'-GAUCCAGUAGGUAGGACAUUU-3'; siTOP3A #1, 5'-CCAGAAAUCUUCCACAG

CellPress
OPEN ACCESS

AA-3'; siTOP3A #2, 5'-GCAGAGAUGUCUAAUGAAA-3'. siBRCA1 #1 is an siPOOL of 30 siRNAs (siTOOLs Biotech), which reduce off-target effects by including very small concentrations of each individual siRNA while still achieving efficient knockdowns with 10-fold less total siRNA concentration compared to single siRNA transfections.[133] siEXO1, siPICH and siSLX4 are Dharmacon SMARTpools (Horizon Discovery); si53BP1 is a Silencer Select siRNA (Thermo Fisher Scientific).

Plasmids and cloning

All plasmids were maxiprepped using GenElute HP Endotoxin-Free Plasmid Maxiprep Kits (Merck) according to the manufacturer's instructions, and verified by Sanger sequencing (Source BioScience). Plasmids encoding GFP-tagged BLM^{WT}, BLM^{K695R} or $BLM^{\Delta TR}$ were generated previously.[17,66]

pDONR221-Spot-BARD1 was produced by amplifying BARD1 cDNA from pDONR221-BARD1[92] by PCR using primers that add the Spot-tag and a short linker to the BARD1 N terminus, and an attB2 to the C terminus. A second round of PCR was carried out to add an N-terminal attB1 site, before cloning the Spot-BARD1 cDNA back into pDONR221 using Gateway cloning (Thermo Fisher Scientific) according to the manufacturer's instructions. The S148A mutation was introduced by site-directed mutagenesis using QuikChange (Agilent Technologies). For immunoprecipitations, Spot-BARD1 cDNAs were amplified by PCR from pDONR221, and subcloned into pcDNA3.1(+). For lentiviral transductions, Spot-BARD1 cDNAs were inserted into pLenti PGK Neo DEST (a gift from Eric Campeau and Paul Kaufman[134]; Addgene plasmid # 19067) using Gateway cloning.

GFP-SLX4 was amplified by PCR from pcDNA5/FRT/TO-GFP-SLX4 (a gift from John Rouse[21]) and inserted into a modified TLCV2 vector (a gift from Philip Hublitz) to replace the Cas9 cassette using In-Fusion cloning (Takara Bio) according to the manufacturer's instructions.

Plasmids expressing mCherry-LacR-BARD1 fusion proteins were produced by amplifying BARD1 cDNA by PCR from pDONR221-Spot-BARD1 and inserting into Cherry-LacRep (a gift from Mirek Dundr[135]; Addgene plasmid # 18985) using In-Fusion cloning according to the manufacturer's instructions.

Plasmids expressing GFP-BRCA1 in a doxycycline-inducible manner were produced by amplifying GFP-BRCA1 cDNA by PCR from pDEST-FRT/TO-GFP-BRCA1 (a gift from Daniel Durocher[136]; Addgene plasmid # 71116) and inserting it into pDONR221 using Gateway cloning. The ΔCC and S1655A mutations were introduced by site-directed mutagenesis. GFP-BRCA1 cDNAs were then inserted into pInducer20 (a gift from Stephen Elledge[137]; Addgene plasmid # 44012) using Gateway cloning.

Generation of knockout cells using CRISPR-Cas9

TP53 was knocked out in RPE-1 FRT/TR cells using an all-in-one CRISPR-Cas9 vector in combination with Nutlin-3 treatment as described previously.[127] *BLM* was knocked out in HCT116 $BARD1^{AID/AID}$ cells using a previously described all-in-one CRISPR-Cas9 vector.[17] To knock out *RECQL5* in RPE-1 FRT/TR cells, small guide RNAs (sgRNAs) were designed targeting the following sequences: sgRECQL5-1, AACAACTTCAATGAAAAGGC; sgRECQL5-2, AGCCCAAAAAGATTCGGGGA. sgRECQL5-1 was cloned into pSpCas9(BB)-2A-GFP (PX458; a gift from Feng Zhang[138]; Addgene plasmid # 48138). sgRECQL5-2 was cloned into a modified PX458 in which the GFP was replaced with mRuby2 (a gift from Philip Hublitz[139]). Plasmids were transfected into cells using Lipofectamine 3000 (Thermo Fisher Scientific), according to the manufacturer's instructions. Cells were left to recover for 3 days before sorting GFP-positive cells (when targeting *BLM*) or GFP- and mRuby2-positive cells (when targeting *RECQL5*). Colonies were grown from single cells and screened for BLM or RECQL5 expression by western blotting.

SDS-PAGE and western blotting

SDS-PAGE and western blotting were performed using 7% Tris-Bicine gels with the SE400 and TE42 systems from Hoefer, or Bolt 4%–12% Bis-Tris Plus gels from Thermo Fisher Scientific. The following antibodies were used at the indicated dilutions: 53BP1 (sc-22760, Santa Cruz Biotechnology, 1/1000), Abraxas (ab139191, Abcam, 1/2000), BARD1 (ab64164, Abcam, 1/500), BARD1 (A300-263A, Bethyl Laboratories, 1/10,000), BLM (A300-110A, Bethyl Laboratories, 1/2000), BRCA1 (sc-6954, Santa Cruz Biotechnology, 1/200), BRCA2 (OP95, Merck, 1/2000), CtIP (ab155988, Abcam, 1/500), EME1 (sc-53275, Santa Cruz Biotechnology, 1/500), ERCC1 (sc-56673, Santa Cruz Biotechnology, 1/500), EXO1 (ab95068, Abcam, 1/2000), FANCJ (4578, Cell Signaling Technology, 1/500), GFP (11814460001, Roche, 1/5000), GST (sc-138, Santa Cruz Biotechnology, 1/500), H2AX (NB100-383, Novus Biologicals, 1/5000), KAP1 (ab10483, Abcam, 1/5000), KAP1-pS824 (IHC-00073, Bethyl Laboratories, 1/1000), MUS81 (sc-53382, Santa Cruz Biotechnology, 1/200), PALB2 (A301-246A, Bethyl Laboratories, 1/2000), PICH (04-1540, Merck, 1/500), RAD51 (70-002, BioAcademia, 1/1000), RECQL5 (A302-520A, Bethyl Laboratories, 1/1000) RMI1 (NB100-1720, Novus Biologicals, 1/1000), RPA2 (ab10359, Abcam, 1/10,000), SLX4 (NBP1-28680, Novus Biologicals, 1/1000), SLX4IP (sc-377066, Santa Cruz Biotechnology, 1/500), TOP3A (14525-1-1AP, Proteintech, 1/1000), XPF (A301-315A, Bethyl Laboratories, 1/1000).

QIBC for RAD51 foci

Cells were grown on 12-mm-wide, 0.13-0.16-mm-thick glass coverslips (VWR; cleaned in 96% ethanol, dried, and autoclaved), irradiated where appropriate using a calibrated Faxitron X-ray generator, pre-extracted with ice-cold 0.2% Triton X-100 in PBS for 1 min on ice, and fixed in 4% formaldehyde in PBS for 12 min at room temperature. Coverslips were incubated for 1 hr at room temperature with anti-RAD51 primary antibody (70-002, BioAcademia, 1/1000), diluted in antibody buffer (DMEM supplemented with 10% FCS and 0.05% sodium azide; filtered). Cells were washed three times in 0.2% Tween 20 in PBS, before incubation with donkey anti-rabbit

IgG Alexa Fluor 568 secondary antibody (A10042, Thermo Fisher Scientific, 1/1000), diluted in antibody buffer containing 0.5 μg/ml DAPI in the dark for 1 hr at room temperature. Cells were washed three times in 0.2% Tween 20 in PBS and once in water, before mounting in 5 μl of a 10% Mowiol 4-88 (Merck), 25% glycerol, 100 mM Tris-HCl, pH 8.5 solution.

QIBC experiments were performed on an Olympus scanR inverted microscope system equipped with IX83 inverted motorized frame with Z-drift control, Semrock DAPI/FITC/Cy3/Cy5 Quad LED filter set, sCMOS Hamamatsu Orca Fusion B Camera (Pixel size on chip 6.5 μm, Array size, 2304 x 2304 pixels or 5.3M pixels, FOV 14.976 mm x 14.976 mm). An Olympus UPLXAPO 20x, NA 0.80, WD 0.6 mm, Air/Dry objective was used. Light sources were Lumencor SPECTRA X Light Engine Independent LEDs (Violet 395/25 295 mW, Yellow 575/25 310 mW, Red 640/30 231 mW) used at 100% power. Identical exposure times were used for all samples within one experiment. Images were captured, processed, and analyzed using scanR acquisition and image analysis software (Olympus, version 3.2.0). A virtual mask was applied for RAD51. Segmentation of nuclei and foci was performed using the in-built object detection module based on intensity and size inclusion criteria. All downstream analyses were performed using TIBCO Spotfire software (version 16.6.0). Fluorescence intensities of the segmented nuclei and foci are depicted as arbitrary units. Cells in S/G2 phase were gated using profiles generated using scatter plots of total DAPI intensity.

Colony survival assays

Where indicated, cells were transfected with siRNA and/or treated with 2 μg/ml doxycycline 24 hr prior to plating at low densities. 24 hr after plating, cells were treated with olaparib, cisplatin and/or 1 mM of the auxin indole-3-acetic acid (IAA) where indicated, for 72 hr. Cells were washed three times in PBS before addition of fresh medium, and left for up to 14 days to allow colonies to develop. Colonies were washed in PBS, stained in 0.1% Coomassie Brilliant Blue R 250, 7% acetic acid, 50% methanol at room temperature for 30 min, and washed in water before counting.

Apoptosis assays

Apoptosis assays were performed using the Caspase-Glo 3/7 Assay System from Promega, according to the manufacturer's instructions. Briefly, cells were treated with either siCtrl or siBRCA1 before being plated into 96-well plates at a density of 5000 cells/well. Medium was replaced 24 hr after plating. 48 hr after transfection, medium was replaced with 100 μl of Caspase-Glo 3/7 Reagent with brief mixing in an orbital shaker for 30 s. Cells were incubated for 30 min at room temperature and luminescence of each well was measured.

Flow cytometry

Cells were transfected with siRNA 48 hr prior to being harvested by trypsinization, pre-extracted in 0.2% Triton X-100 in PBS for 10 min on ice, and fixed using BD Cytofix/Cytoperm solution (BD Biosciences) according to the manufacturer's instructions. Cells were labelled with γH2AX antibodies (05-636, Millipore, 1/500) diluted in BD Perm/Wash buffer (BD Biosciences) for 1 hr at room temperature, followed by incubation with goat anti-mouse IgG1 Alexa Fluor 647 secondary antibodies (A21240, Thermo Fisher Scientific, 1/200), 250 μg/ml RNase A (Merck), 0.02% sodium azide and 2 μg/ml DAPI, diluted in BD Perm/Wash buffer for 1 hr at room temperature in the dark. Samples were resuspended in BD Perm/Wash buffer for analysis. γH2AX intensities were normalized by subtracting the γH2AX intensity of untreated WT cells from every sample.

Micronuclei quantification

Cells were fixed in 4% paraformaldehyde in PBS for 10 min at room temperature, washed twice with PBS, permeabilized and blocked in blocking buffer (3% BSA, 0.5% Triton X-100 in PBS) for 30 min at room temperature. Coverslips were washed in PBS, then incubated with anti-human centromere primary antibody (HCT-0100, Immunovision, 1/1000) in antibody buffer for 1 hr at room temperature. Cells were washed three times in 0.2% Tween 20 in PBS, before incubation with goat anti-human IgG Cy3 secondary antibody (109-165-003, Jackson ImmunoResearch, 1/1000), diluted in antibody buffer containing 0.5 μg/ml DAPI in the dark for 1 hr at room temperature. Cells were washed three times in 0.2% Tween 20 in PBS and once in water, before mounting in 5 μl of a 10% Mowiol 4-88 (Merck), 25% glycerol, 100 mM Tris-HCl, pH 8.5 solution. Images were obtained using the Olympus scanR inverted microscope system as above, from which micronuclei were scored manually.

Analyses of chromosomal aberrations

HCT116 or RPE-1 cells were blocked in mitosis by addition of 750 nM colchicine for 2 hr before harvesting. Cells were resuspended in 75 mM KCl and incubated at 37 °C for 30 min, followed by fixation by addition of ice-cold 3:1 methanol/acetic acid solution. Following gentle inversion and centrifugation, pellets were resuspended in fixative and spun down, with this procedure being repeated twice. Pellets were then resuspended in fixative, and cells were dropped onto glass slides (VWR) that had been pre-treated with 0.432% HCl for 1 hr, washed six times in water, and stored in ethanol. Cells were left to dry at room temperature for up to 3 days in the dark, before staining by immersion in Giemsa Modified Stain (Merck) in Gurr Buffer (Thermo Fisher Scientific) for 10 min. Cells were rinsed in water and left to dry overnight in the dark before mounting in Entellan (Merck) with glass coverslips (Appleton Woods). Images were acquired using an Olympus BX60 widefield microscope fitted with a Lumenera INFINITY3S camera and a UPlanSApo 100x/1.4 oil objective. At least 10 metaphases were scored per sample.

CellPress
OPEN ACCESS

Lentiviral transductions

To assemble lentiviruses, 293FT cells were transfected with pLenti PGK Neo DEST plasmids encoding GFP, GFP-BLM or BARD1 proteins, TLCV2 plasmids encoding GFP-SLX4, or pInducer20 plasmids encoding GFP or GFP-BRCA1 proteins, along with pHDM-tat1b, pHDM-G, pRC/CMV-rev1b and pHDM-Hgpm2 lentiviral assembly plasmids.[140] Viral supernatants were harvested at 24 and 48 hr, pooled, passed through a 0.45-μm filter, and stored at -80 °C. For lentiviral infections, HCT116 or RPE-1 cells were incubated in viral media for 48 hr, before selection in fresh medium containing 500 μg/ml G418 or 1 μg/ml puromycin for up to 7 days. G418-resistant cells were sorted for GFP expression where possible. All stable cell lines were verified by western blotting.

TCGA analyses

The TCGA Pan-Cancer dataset (12,839 samples) was used for this study. Tumour samples that do not contain information of gene expression level were excluded. The UCSC Xena platform[141] was used for acquiring gene expression levels (FPKM) of BTR complex components (*BLM*, *TOP3A*, *RMI1* and *RMI2*) and known synthetic lethal partners (*POLQ* and *PARP1*) in tumour samples with WT *BRCA1* (8,221 samples) and loss-of-function (LoF) alterations (33 samples). The LoF alterations in this study only include frameshift and nonsense mutations. A similar approach was used to compare FPKM of *BLM* in breast, ovarian, pancreatic, and prostate tumour samples with mutations in *BRCA1* or *BRCA2*. Welch's t-test was applied for comparing gene expression levels between tumour samples.

Sequence alignments

Protein sequences were aligned using T-Coffee,[131] with conserved and similar residues highlighted using pyBoxshade.

Peptide pull-downs

Peptides were synthesized by Biomatik or Genosphere Technologies and biotinylated on the N terminus with the following sequences: SGSG-KNSIKMWFSPRSKKVRYVVSK (BARD1-S148), SGSG-KNSIKMWF-[pSer]-PRSKKVRYVVSK (BARD1-pS148), SGSG-TKSRNEVVTPEKVCKNYLTSK (BARD1-T299), SGSG-TKSRNEVV-[pThr]-PEKVCKNYLTSK (BARD1-pT299), and SGSG-LPLSQNSASELPASQPQPFS (RAD17). Peptides were bound to streptavidin-coupled Dynabeads M-280 (Thermo Fisher Scientific). HeLa nuclear extracts (Ipracell) were diluted 1:1 with dilution buffer (300 mM NaCl, 10 mM NaF, 0.2 mM EDTA, 0.2% Igepal CA-630, 20 mM HEPES-KOH, pH 7.4) supplemented with cOmplete protease inhibitor cocktail (Roche), and cleared by centrifugation. For preparation of 293, 293FT and U2OS lysates, cells were washed in phosphate-buffered saline (PBS), lysed in peptide pull-down buffer (150 mM NaCl, 50 mM KCl, 5 mM NaF, 0.2 mM EDTA, 0.1% Igepal CA-630, 10% glycerol, 20 mM HEPES-KOH, pH 7.4) supplemented with cOmplete protease inhibitor cocktail, before being were cleared by centrifugation. Dynabead-conjugated peptides were incubated with clarified extracts with end-to-end mixing at 4 °C for 2 hr. Beads were washed with peptide pull-down buffer, before elution in 2X SDS sample buffer (4% SDS, 20% glycerol, 50 mM TCEP, 0.002% bromophenol blue, 125 mM Tris-HCl, pH 6.8) for mass spectrometry or western blotting.

Circular dichroism spectroscopy

Circular dichroism spectroscopy was performed using a Jasco J-815 Spectropolarimeter. BARD1-S148 and BARD1-pS148 peptides were diluted in 20 mM NaCl, 10 mM sodium phosphate buffer (pH 6.8) at a final concentration of 50 μg/ml. Peptides were applied to 1-mm cuvettes for working in the far-UV spectrum (190-230 nm). Buffer without peptide was used to set a baseline. Experimental data was reconstructed, and secondary structure fractions were calculated using a reference database[142] and DichroWeb.[132]

Mass spectrometry

Precipitated material in SDS sample buffer was subjected to two rounds of chloroform-methanol precipitation followed by in-solution trypsin digestion. Digested and desalted samples were resuspended in 20 μl 2% acetonitrile and 0.1% formic acid and analyzed by reverse-phase chromatography using an UltiMate 3000 nUPLC with a 50-cm EASY-Spray column and a 2-cm Acclaim PepMap 100 column connected either to a Q-Exactive HF mass spectrometer or an Orbitrap Fusion Lumos mass spectrometer through an EASY-Spray Ion Source (Thermo Fisher Scientific). Peptides were separated using a 60-min linear gradient from 2% to 35% buffer containing formic acid in acetonitrile at 250 nl/min flow rate. Both mass spectrometers were operated in data-dependent acquisition mode to switch automatically between full scan and MS/MS acquisition. For the Q-Exactive HF (experiment 2, E2), MS1 scans were acquired in the Orbitrap at 60k resolution (AGC 3e6) and the top 12 most intense precursors were isolated in the quad (1.2 m/z window), fragmented in the HCD cell with 28% normalized collision energy and analysed in the Orbitrap at 30k. For the Orbitrap Fusion Lumos (experiment 1, E1), the top speed universal method was used. MS1 scans were acquired in the Orbitrap (AGC target of 4e5 and S-lens RF of 30) at 120k and MS2 scans in the ion trap using the rapid scan mode (quad isolation 1.6 m/z, CID 35%, activation time 10 ms). Mass spectrometry data were analysed in FragPipe (v19). Data were searched against the UniProtKB/Swiss-Prot database (human, retrieved 02/2022, 20,386 sequences) and quantified using the LFQ-MBR workflow. FragPipe combined-protein outputs were further analysed in Perseus (v1.6.2.2). For each experiment, protein intensity ratios of BARD1-pS148 versus BARD1-S148 were calculated, $\log_2$ transformed and missing values replaced by a constant (equal to 0). E1 and E2 data were merged based on the

gene name and combined total peptide average between the two experiments was calculated. The mass spectrometry proteomics data have been deposited to the ProteomeXchange Consortium via the PRIDE[143] partner repository with the dataset identifier PXD042480.

Immunoprecipitations

Plasmids were transfected into 293FT cells using Lipofectamine 2000 (Thermo Fisher Scientific) according to the manufacturer's instructions. For preparation of lysates for immunoprecipitations, cells were washed in phosphate-buffered saline (PBS), and lysed in nuclease buffer (100 mM NaCl, 0.1% Igepal CA-630, 1 mM $MgCl_2$, 10% glycerol, 5 mM NaF, 50 mM Tris-HCl, pH 7.5), supplemented with cOmplete EDTA-free protease inhibitor cocktail and 25 U/ml Benzonase. After nuclease digestion, NaCl and EDTA concentrations were adjusted to 300 mM and 2 mM, respectively, and lysates were cleared by centrifugation. Lysates were then incubated with 15 μl of Spot-Trap magnetic agarose beads (Proteintech) for 2 hr with end-to-end mixing at 4 °C. Immunoglobulin-antigen complexes were washed five times in wash buffer (750 mM NaCl, 2 mM EDTA, 0.1% Igepal CA-630, 10% glycerol, 5 mM NaF, 50 mM Tris-HCl, pH 7.5) supplemented with cOmplete EDTA-free protease inhibitor cocktail, before elution in 2X SDS sample buffer for SDS-PAGE.

LacR/*lacO* single-cell colocalization assays

U2OS 2-6-3 cells containing an integrated array of ~256 *lacO* repeats were grown on 12-mm-wide, 0.13-0.16-mm-thick glass coverslips (VWR; cleaned in 96% ethanol, dried, and autoclaved). Cells were co-transfected with pcDNA5/FRT/TO-GFP-SLX4 and either mCherry-LacR, mCherry-LacR-BARD1^{WT} or mCherry-LacR-BARD1^{S148A}. The following day, cells were mock-treated or treated with 9 μM of the CDK1 inhibitor RO-3306 for 1 hr before fixation for immunofluorescence and microscopy.

Sister chromatid exchange assays

HCT116 or RPE-1 cells were treated with 10 μM 5-bromo-2'-deoxyuridine (BrdU) for two cell cycles, arrested at the G2/M boundary by 9 μM CDK1 inhibitor (RO-3306) treatment for 16 hr, and blocked in mitosis by addition of 750 nM colchicine for up to 2 hr before harvesting. Cells were resuspended in 75 mM KCl and incubated at 37 °C for 30 min, followed by fixation by addition of ice-cold 3:1 methanol/acetic acid solution. Following gentle inversion and centrifugation, pellets were resuspended in fixative and spun down, with this procedure being repeated twice. Pellets were then resuspended in fixative, and cells were dropped onto glass slides (VWR) that had been pre-treated with 0.432% HCl for 1 hr, washed six times in water, and stored in ethanol. Cells were left to dry at room temperature for up to 3 days in the dark, before staining by immersion in 15 μg/ml Hoechst diluted in 100 mM phosphate buffer (51 mM NaH_2PO_4, 49 mM Na_2HPO_4, pH 6.8) for 30 min. Cells were washed in PBS, exposed to a 365-nm UV light source for 2 hr, and washed again in PBS. This was followed by incubation in 2X saline-sodium citrate (SSC) buffer (300 mM NaCl, 30 mM trisodium citrate-HCl, pH 7) for 1 hr at 65 °C and four washes in water. Cells were stained with Leishman's stain (Merck) for 90 s and left in the dark for 30 min to dry. Cells were then washed once in water, left to dry overnight in the dark before mounting in VECTASHIELD (Vector Laboratories) with glass coverslips (Appleton Woods). Images were acquired using a ZEISS Axio Observer Z1 widefield microscope fitted with an Axiocam MRm camera and a Plan-Apochromat 100x/1.4 oil objective, running on ZEN Pro 2012 software. At least 10 metaphases were scored per sample.

Immunofluorescence and confocal microscopy

Cells were grown on 12-mm-wide, 0.13-0.16-mm-thick glass coverslips (VWR; cleaned in 96% ethanol, dried, and autoclaved). Cells were treated with 2 μg/ml doxycycline 16 hr after siRNA transfection. The following day, cells were treated with 1 mM IAA for 8 hr where indicated, before addition of 200 nM aphidicolin for 16 hr, followed by 100 ng/ml nocodazole for 1 hr to enrich for mitotic cells. Cells were fixed in 4% paraformaldehyde in PBS for 10 min at room temperature, washed twice with PBS, permeabilized and blocked in blocking buffer (3% BSA, 0.5% Triton X-100 in PBS) for 30 min at room temperature. Coverslips were washed in PBS, then incubated with anti-GFP (11814460001, Roche, 1/2000) or anti-MUS81 (sc-53382, Santa Cruz Biotechnology, 1/1000) primary antibodies in antibody buffer for 1 hr at room temperature. Cells were washed three times in 0.2% Tween 20 in PBS, before incubation with goat anti-mouse IgG Alexa Fluor Plus 488 secondary antibody (A32723, Thermo Fisher Scientific, 1/1000), diluted in antibody buffer containing 0.5 μg/ml DAPI in the dark for 1 hr at room temperature. Cells were washed three times in 0.2% Tween 20 in PBS and once in water, before mounting in 5 μl of a 10% Mowiol 4-88 (Merck), 25% glycerol, 100 mM Tris-HCl, pH 8.5 solution.

Confocal imaging was carried out using a Leica SPE microscope (Leica Microsystems) equipped with a 63x/1.3 NA Plan Apochromat objective. DAPI was detected using a 405-nm diode laser, Alexa 488 was detected with the 488-nm line of an argon laser, Z stacks of entire cells were acquired using optimized step sizes by LAS X software. Raw data were processed using Projection processing with LAS X software. Display of images was adjusted for intensity for optimal display of structures of interest.

QUANTIFICATION AND STATISTICAL ANALYSIS

Unless otherwise stated, significances were calculated using one-way ANOVA, followed by Tukey's post-hoc test.